Published June 8, 2015

KCC2 regulates actin dynamics in dendritic spines via interaction with β-PIX

Olaya Llano,[1] Sergey Smirnov,[1] Shetal Soni,[1] Andrey Golubtsov,[1] Isabelle Guillemin,[4] Pirta Hotulainen,[1] Igor Medina,[2,3] Hans Gerd Nothwang,[4] Claudio Rivera,[1,2,3] and Anastasia Ludwig[1]

[1]Neuroscience Center, University of Helsinki, FI-00014 Helsinki, Finland
[2]Institut de Neurobiologie de la Méditerranée, Institut National de la Santé et de la Recherche Médicale Unité 901, 13009 Marseille, France
[3]Aix-Marseille Université, Unité Mixte de Recherche 901, 13273 Marseille, France
[4]Neurogenetics group, Center of Excellence Hearing4All, School of Medicine and Health Sciences and Research Center for Neurosensory Sciences, Carl von Ossietzky University Oldenburg, 26111 Oldenburg, Germany

Chloride extrusion in mature neurons is largely mediated by the neuron-specific potassium-chloride cotransporter KCC2. In addition, independently of its chloride transport function, KCC2 regulates the development and morphology of dendritic spines through structural interactions with the actin cytoskeleton. The mechanism of this effect remains largely unknown. In this paper, we show a novel pathway for KCC2-mediated regulation of the actin cytoskeleton in neurons. We found that KCC2, through interaction with the b isoform of Rac/Cdc42 guanine nucleotide exchange factor β-PIX, regulates the activity of Rac1 GTPase and the phosphorylation of one of the major actin-regulating proteins, cofilin-1. KCC2-deficient neurons had abnormally high levels of phosphorylated cofilin-1. Consistently, dendritic spines of these neurons exhibited a large pool of stable actin, resulting in reduced spine motility and diminished density of functional synapses. In conclusion, we describe a novel signaling pathway that couples KCC2 to the cytoskeleton and regulates the formation of glutamatergic synapses.

Introduction

Development of neuronal networks in the brain requires synchronized maturation of excitatory and inhibitory neurotransmission. The neuron-specific potassium-chloride cotransporter KCC2 has been suggested as a synchronizing factor (Li et al., 2007). KCC2 is critically involved in the development of inhibitory neurotransmission (Rivera et al., 1999; Hübner et al., 2001; Payne et al., 2003) as well as in the development of excitatory, glutamatergic synapses (Li et al., 2007; Gauvain et al., 2011) and the maturation of dendritic spines, where most of the glutamatergic synapses are located (Gulyás et al., 2001; Li et al., 2007; Fiumelli et al., 2013).

The morphology of dendritic spines is essentially sustained by a branched network of actin filaments controlled by actin binding proteins and regulated through multiple signaling cascades (Matus et al., 1982; Honkura et al., 2008; Hotulainen et al., 2009; Penzes and Cahill, 2012; Saneyoshi and Hayashi, 2012). Important regulators of actin polymerization are small GTPases of the Rho family. Small GTPase Rac1 is activated by guanine-nucleotide exchange factors (GEFs), including the GEF β-PIX in complex with p21-activated kinase (PAK). The activation of Rac1 triggers a cascade resulting in LIM-kinase–mediated phosphorylation of the actin-depolymerizing factor ADF/cofilin (Manser et al., 1998; Edwards et al., 1999; Bokoch, 2003). Phosphorylation inactivates ADF/cofilin and leads to the stabilization of the actin cytoskeleton inside spines (Sarmiere and Bamburg, 2004).

Morphogenesis of dendritic spines requires substantial dynamic rearrangements of the actin cytoskeleton (Calabrese et al., 2006). Although the role of KCC2 in spine and synapse development has been intensively studied (Gulyás et al., 2001; Li et al., 2007; Gauvain et al., 2011; Fiumelli et al., 2013), whether KCC2 affects actin dynamics in spines remains obscure.

In this study, we demonstrate that KCC2-deficient neurons exhibit increased stability of actin filaments in dendritic spines and a high level of cofilin-1 phosphorylation. Cofilin-1 phosphorylation as well as actin dynamics can be restored by expression of chloride-transport-deficient mutants of KCC2, suggesting that KCC2 regulates actin dynamics in a chloride-transport-independent manner. In our search for putative interacting partners, we found that KCC2, through its C-terminal domain (CTD), binds β-PIXb and inhibits its GEF activity toward Rac1, leading to a decrease in cofilin-1

Correspondence to Claudio Rivera: claudio.rivera@helsinki.fi; or Anastasia Ludwig: anastasia.ludwig@helsinki.fi

Abbreviations used in this paper: ANOVA, analysis of variance; co-IP, coimmunoprecipitation; CTD, C-terminal domain; DIV, day in vitro; FRET, Förster resonance energy transfer; GEF, guanine nucleotide exchange factor; KO, knockout; mEPSC, miniature excitatory postsynaptic current; PAK, p21-activated kinase; VGLUT1, vesicular glutamate transporter-1; WT, wild type.

Supplemental Material can be found at:
http://jcb.rupress.org/content/suppl/2015/06/04/jcb.201411008.DC1.html

The Rockefeller University Press $30.00
J. Cell Biol. Vol. 209 No. 5 671–686
www.jcb.org/cgi/doi/10.1083/jcb.201411008

Published June 8, 2015

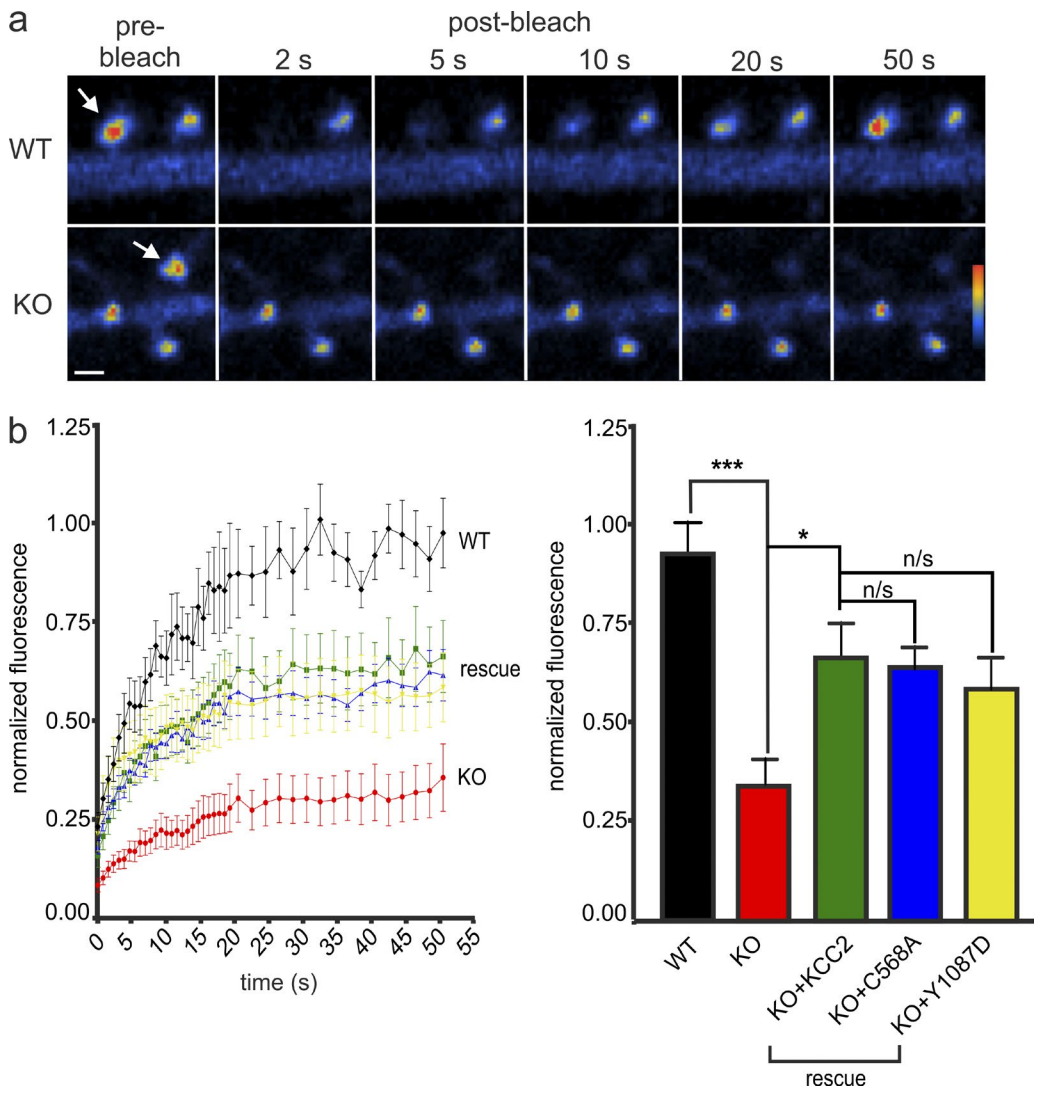

Figure 1. **KCC2-deficient neurons show reduced actin turnover.** (a) FRAP. Time-lapse images of KCC2 KO and WT hippocampal cells. The fluorescence of GFP-actin is highlighted by pseudocolor; arrows indicate bleached spines. Bar, 2 µm. (b, left) Averaged FRAP curves. Rate of actin turnover in spines from KCC2 KO neurons (KO, red) and KCC2 WT neurons (WT, black) as well as from KO neurons overexpressing KCC2 (green curve) and the KCC2 mutants C568A (blue) and Y1087D (yellow). (right) Normalized fluorescence recovery of GFP-actin at 48 s after bleach. (6–13 spines per condition; one-way analysis of variance [ANOVA], Tukey–Kramer post-test; *, $P < 0.05$; ***, $P < 0.001$; not significant [n/s], $P > 0.05$.) Error bars indicate SEM.

phosphorylation level. Furthermore, we demonstrate that in neurons, KCC2 controls glutamatergic synaptogenesis through the regulation of β-PIX activity. In summary, in this study, we establish a novel pathway in which KCC2 regulates actin dynamics via the Rac1/β-PIX/cofilin cascade, leading to the formation of glutamatergic synapses.

Results

Genetic ablation of KCC2 dramatically increases stability of actin filaments in dendritic spines

Premature or ectopic expression of KCC2 affects the structure of the actin cytoskeleton in developing neurons (Horn et al., 2010) and in cancer cells (Wei et al., 2011). Here, we studied whether KCC2 regulates actin dynamics in dendritic spines. We used FRAP technique to assess actin treadmilling in dendritic spines (Star et al., 2002; Koskinen et al., 2012) of days in vitro (DIV) 15–17 KCC2 knockout (KO; Tornberg et al., 2005) and wild-type (WT) dissociated hippocampal neurons overexpressing β-actin fused to GFP. Both WT and KO neurons developed spines of various morphologies; thus, all spines analyzed were chosen in a random manner irrespective of their type. We found that in spines of WT neurons the recovery of the fluorescence intensity after the bleach was close to 100% within 1 min (Fig. 1, a and b). In contrast, postbleach fluorescence in spines of KO neurons recovered to ∼35% of the initial level, indicating that the stable pool of actin was substantially higher in KO spines than in WT spines. To verify that KCC2 deficiency was responsible for this dramatic phenotype, we overexpressed KCC2b in KO neurons and observed restoration of actin dynamics (∼60% of the initial level; Fig. 1 b). The restoration was not complete, which may indicate that chronic lack of KCC2 produces additional long-term effects that cannot be fully recovered by short-term expression of KCC2b.

Published June 8, 2015

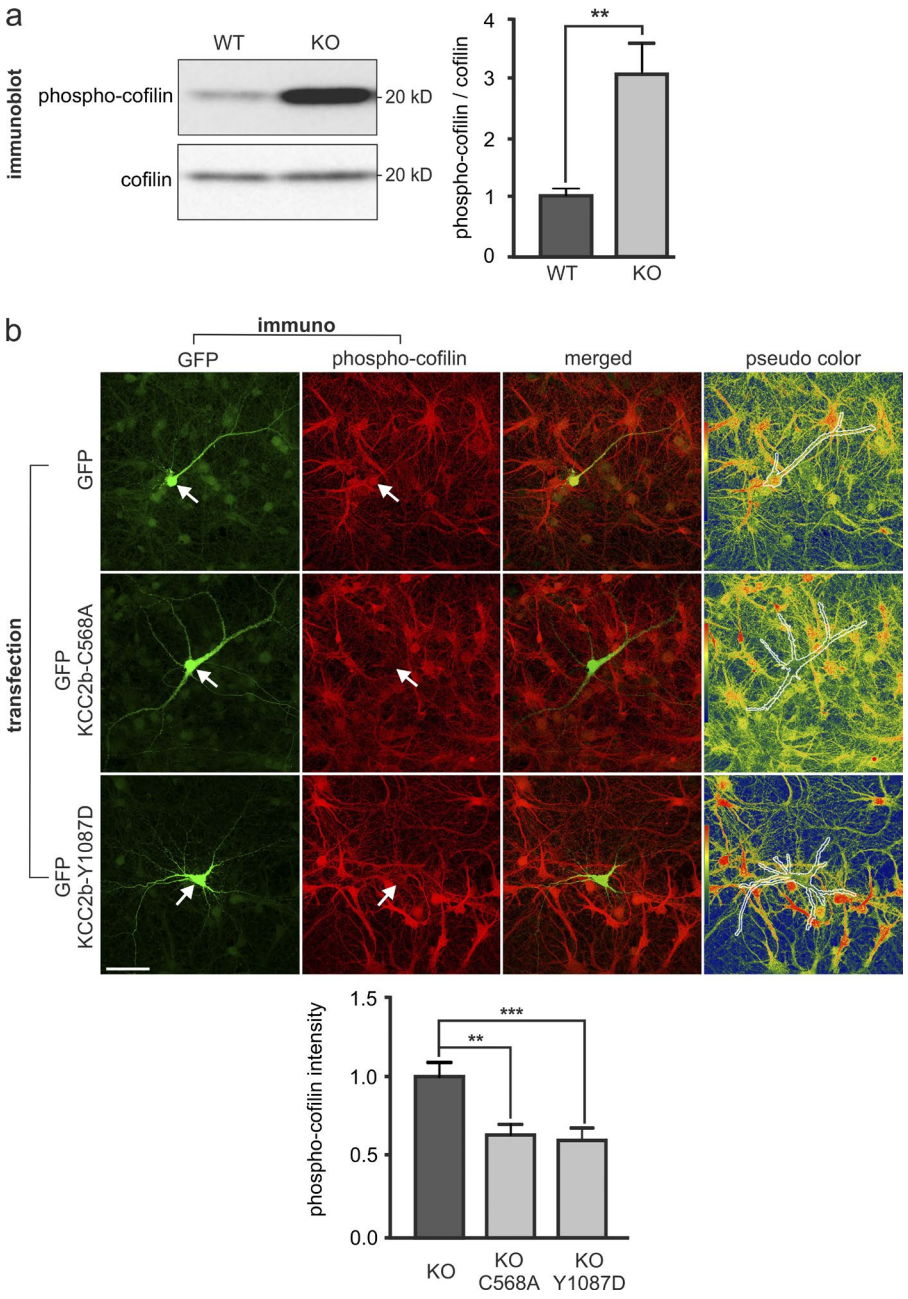

Figure 2. **Cofilin-1 is highly phosphorylated in the absence of KCC2.** (a, left) Immunoblot of neuronal cultures from KCC2 KO mice and WT littermates with anti-phospho-cofilin and anti-cofilin antibodies. (right) Quantification of the phospho-cofilin/cofilin ratio (cultures from 5–7 embryos; unpaired *t* test, P = 0.0086.) Error bars indicate SEM. (b, top) Immunostaining of KCC2 KO hippocampal neurons overexpressing GFP alone, GFP and KCC2b-C568A, as well as GFP and KCC2b-Y1087D with anti-phospho-cofilin antibodies (red and pseudocolor). Arrows indicate transfected neurons. Bar, 50 µm. (bottom) Quantification of immunofluorescence in transfected neurons (28–30 cells per condition; Kruskal–Wallis test, Dunn's post-test; **, P < 0.01; ***, P < 0.001.) Error bars indicate SEM.

Next, we overexpressed, in KO neurons, KCC2 mutants incapable of chloride transport: KCC2b-C568A (Reynolds et al., 2008) and KCC2b-Y1087D (Strange et al., 2000). Both mutants were well expressed in neurons (Fig. S1 a). Importantly, in FRAP experiments, expression of either of these mutants restored actin turnover to the same level as WT-KCC2b (Fig. 1 b). These data demonstrate that the effect of KCC2 on actin treadmilling is independent of its chloride-extruding activity.

KCC2 regulates the actin cytoskeleton through cofilin-1 phosphorylation

Cofilin-1 is an important actin-depolymerizing factor that is inactivated by phosphorylation at serine 3 (Mizuno, 2013). We assessed cofilin phosphorylation by immunoblotting and found that cultured KCC2 KO neurons at DIV 21 exhibit threefold elevated levels of the phosphorylated form of cofilin-1 when compared with WT neurons (Fig. 2 a). High level of cofilin-1 phosphorylation may be the reason for the increased stability of actin filaments observed in KO neurons (Fig. 1, a and b).

Because augmented phosphorylation of cofilin-1 may be an indirect consequence of altered chloride regulation in KO neurons, we performed rescue experiments with the chloride-transport-deficient mutants of KCC2. We analyzed phospho-cofilin levels by immunostaining and observed that KO neurons expressing either KCC2-C568A or KCC2-Y1087D had significantly lower levels of phospho-cofilin when compared with KO neurons expressing GFP (Fig. 2 b). These results demonstrate that the regulation of cofilin-1 phosphorylation by KCC2 is mainly independent of the chloride extrusion activity of the cotransporter.

KCC2 interacts with β-PIXb

We searched for proteins that may mediate the effect that KCC2 exerts on cofilin-1 phosphorylation and stability of actin cyto-

Published June 8, 2015

skeleton. Using a yeast two-hybrid system, we identified the b isoform of β-PIX (β-PIXb) as a potential KCC2-interacting protein (Fig. S2 a). β-PIXb, a guanine nucleotide exchange factor (GEF) for small GTPases Rac1 and Cdc42, is expressed exclusively in neurons (Kim et al., 2000), in which it acts as a component of the intracellular cascade regulating actin polymerization in dendritic spines (Saneyoshi et al., 2008). Notably, one of the effectors of this cascade is cofilin-1. β-PIXb appears to have preference for KCC2 in comparison to other members of the cation-chloride cotransporter family as suggested by the much weaker β-galactosidase expression displayed by KCC1, KCC3, KCC4, and NKCC1 in comparison to KCC2 (Fig. S2 a).

We assessed the interaction of endogenous KCC2 and β-PIX in adult mouse brain by coimmunoprecipitation (co-IP) assay. We found that anti–β-PIX antibodies pull down complexes of β-PIX and KCC2 from the crude native membrane preparations, indicating the interaction between the endogenous proteins (Fig. 3 a). The assay specificity was confirmed by reprobing the co-IP Western blot membranes with anti-PAK and anti-PSD95 antibodies used as positive and negative controls, respectively. In these experiments, we could also detect previously reported β-PIX–PAK complexes (Zhang et al., 2003). In contrast, anti-PSD95 antibodies detected PSD95 signal in the input but not in the co-IP fraction. Thus, our data strongly suggest specific interaction between KCC2 and β-PIX in brain tissue.

To further characterize β-PIXb–KCC2 interaction, we performed co-IP of exogenously expressed KCC2b and β-PIXb in HEK293T cells. Co-IP confirmed the interaction, as β-PIXb was pulled down together with KCC2b by the anti-KCC2 antibody from the lysate of double-transfected cells (Fig. 3 b, left). Importantly, β-PIXb was not precipitated from the lysates of control cells that expressed either KCC2b or β-PIXb separately. Neither was β-PIXb precipitated from the lysates of control cells that were mixed after the cell lysis procedure, implying that the interaction occurred only in the context of live, intact cells.

In the next series of co-IP experiments, we used anti–β-PIX antibody and lysates of HEK293T cells transfected with β-PIXb and the CTD of KCC2 (KCC2-CTD, amino acids 845–1,116). Similarly to the previous experiment, KCC2-CTD was precipitated together with β-PIXb from the lysate of double-transfected cells (Fig. 3 b, right). No KCC2-CTD band was detected in precipitates from the control lysates. We concluded that KCC2b and β-PIXb interact both in native environments as well as in heterologous expression system, and the interaction involves the CTD of KCC2.

The C terminus of KCC2, along with other KCC isoforms, bears a conserved proline-rich motif that represents a noncanonical recognition site for proteins with SH3 (SRC homology 3) domains. This motif was shown to mediate direct interaction of KCC3 with Vav2, a GEF for Rho family GTPases (Salin-Cantegrel et al., 2013). Because β-PIX is an SH3 domain–containing protein, we tested whether the proline-rich motif at KCC2 C terminus is crucial for KCC2–β-PIX interaction. Of note, mutation of the proline-rich motif in KCC2 does not disrupt its interaction with β-PIXb (Fig. S2 b).

KCC2 inhibits β-PIX–induced activation of Rac1 in HEK cells

Next, we addressed whether interaction of KCC2 and β-PIX influences β-PIX functionality. β-PIX activates Rac1 GTPase by catalyzing the exchange of GDP to GTP (Manser et al., 1998). By means of G-LISA, a small GTPase activation assay, we determined the level of activated Rac1 in HEK293T cells overexpressing Rac1 (control cells) as well as Rac1 together with KCC2b and β-PIXb (Fig. 3 c). As expected, expression of β-PIXb significantly increased the level of Rac1 activation in comparison to control cells. In contrast, expression of KCC2b had no effect on Rac1 activation, indicating that KCC2 cannot directly affect Rac1 activity in HEK293T cells that do not express β-PIXb endogenously. However, when KCC2b was coexpressed with β-PIXb, the β-PIX–induced activation of Rac1 was fully abolished. Importantly, the level of β-PIXb was not affected by coexpression with KCC2b (Fig. S2 d). Thus, coexpression of KCC2b and β-PIXb leads to significant reduction of β-PIX GEF activity toward Rac1.

KCC2 and β-PIXb regulate cofilin-1 phosphorylation in HEK cells

β-PIX forms part of the Rac/PAK/cofilin signaling cascade that leads to phosphorylation of cofilin-1 (Saneyoshi et al., 2008; Saneyoshi and Hayashi, 2012). Having shown that KCC2 interacts with β-PIX and inhibits its GEF activity, we next addressed whether this alters phosphorylation of cofilin-1.

We found that in HEK293T cells neither β-PIXb nor KCC2b overexpression alone caused any significant changes in cofilin-1 phosphorylation (Fig. 3 d). Importantly, when β-PIXb and KCC2b were coexpressed in cells, cofilin-1 phosphorylation was greatly reduced. This observation demonstrates that KCC2 and β-PIX act synergistically to regulate phosphorylation of cofilin-1.

The results presented in Fig. 3 indicate that KCC2b structurally and functionally interacts with β-PIXb, and, in HEK293T cells, this interaction leads to modulation of Rac1 and cofilin-1 activity. Because both Rac1 and cofilin-1 are known to regulate synaptogenesis in neurons (Meng et al., 2002; Tolias et al., 2011), in the second part of our study, we performed several experiments to clarify the role of KCC2 and β-PIX in the maturation of dendritic spines and glutamatergic synapses.

KCC2 inhibits β-PIXb–induced activation of Rac1 in neurons

We assessed β-PIX activity in neurons by Förster resonance energy transfer (FRET) analysis of DIV 7–9 dissociated hippocampal cultures, transfected with Raichu-Rac1, a ratiometric probe that responds to activation of Rac1 GEFs with increased FRET signal (Itoh et al., 2002). We observed FRET signal in cell bodies, neurites, and dendritic spines of transfected cells (Fig. 4 a). To avoid possible indirect consequences of KCC2 overexpression on neuronal excitability, we used the chloride transport–incapable KCC2-C568A mutant in this and all subsequent experiments performed in neurons. Importantly, KCC2b-C568A interacted with β-PIXb to the same extent as nonmutated KCC2 (Fig. S2 c). Overexpression of β-PIXb caused significant increase in FRET (Fig. 4 b) that was fully abolished by coexpression of β-PIXb with KCC2b-C568A. Of note, coexpression with KCC2b-C568A did not affect β-PIXb expression level (Fig. S1 b). This result indicates that KCC2 inhibits β-PIX GEF activity in neurons, as in HEK293T cells. Expression of KCC2b-C568A alone also reduced FRET signal, presumably as a result of attenuation of endogenous β-PIX activity. It is confirmed by the fact that expression of KCC2b-C568A has no effect on FRET signal in the presence of the dominant-negative β-PIXb–DHm (mutated Dbl homology do-

Published June 8, 2015

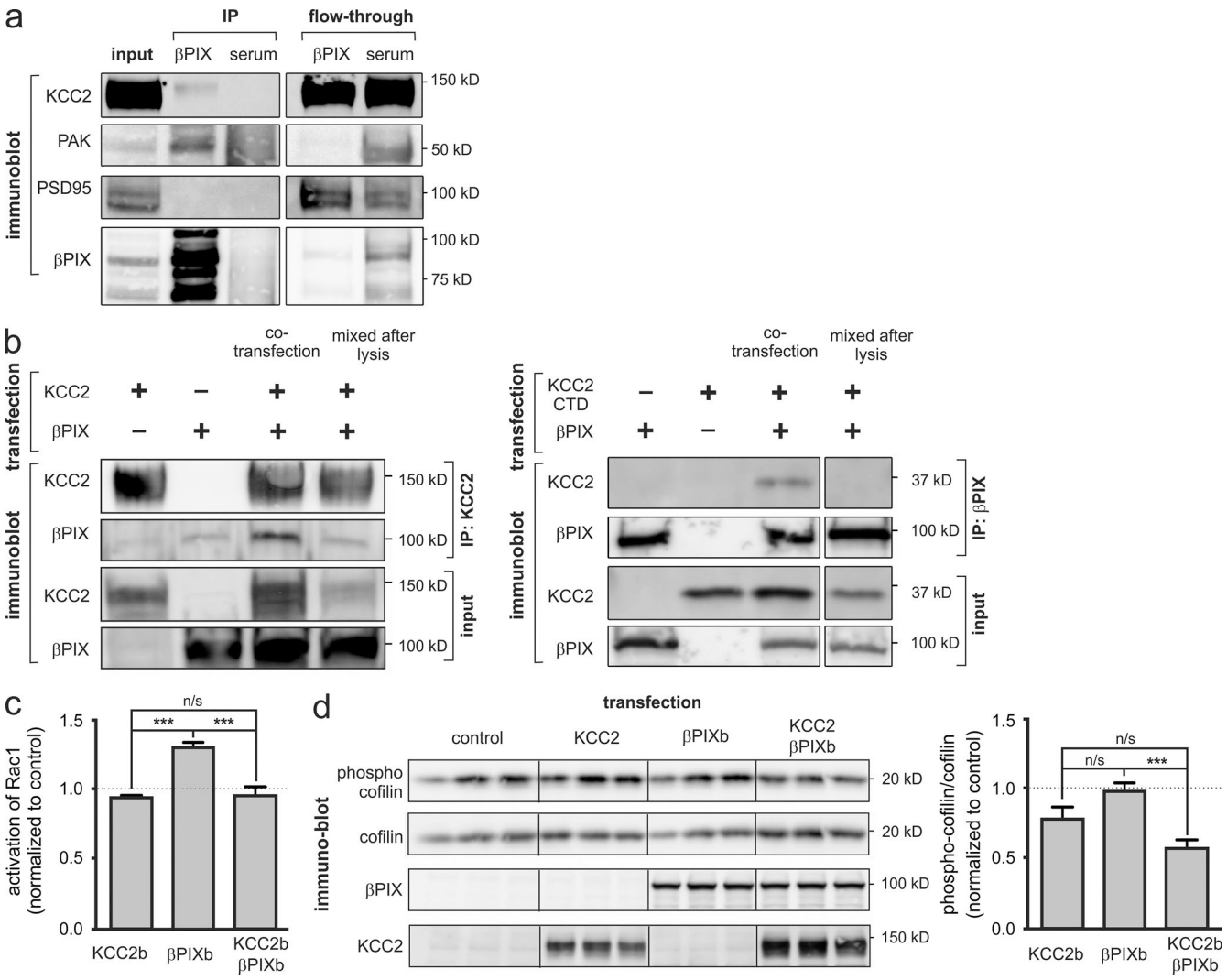

Figure 3. **Interaction of KCC2 with β-PIXb mediates the regulation of Rac1 and cofilin-1 activity.** (a) Immunoblot of the samples from co-IP of endogenous proteins in adult WT male mice brains. Solubilized membrane homogenates (input fraction) were subjected to precipitation with anti–β-PIX antibodies. The eluates resulting from immunoprecipitation (IP fraction) were probed for KCC2b, demonstrating the interaction of KCC2 and β-PIX in adult brains. Reprobing the membrane with anti-PAK1/2/3 antibodies confirmed β-PIX interaction with PAK1 and served as a positive control for co-IP, whereas the anti-PSD95 antibody revealed the absence of the interaction between β-PIX and PSD95 and served as negative control. Flow through shows the unbound fraction. Representative example of two independent biological replicates. (b, left) Immunoblot of the immunoprecipitates from HEK293T cell homogenates expressing KCC2b and/or β-PIXb using antibodies against KCC2 (immunoprecipitation: KCC2) followed by immunoblot detection of β-PIX. The immunoprecipitation yielded β-PIX as interacting partner of KCC2. (right) Immunoblot of the immunoprecipitates from HEK293T cell homogenates expressing the CTD of KCC2b (aa 845–1,116) and/or β-PIXb using anti–β-PIX antibodies (immunoprecipitation: β-PIX) followed by immunoblot detection of KCC2. The last lane of the same membrane (mixed after lysis) is shown separately. Each immunoblot image is a representative example of three independent experiments. (c) G-LISA analysis of Rac1 activation in HEK293T cells expressing Rac1 as well as KCC2b and/or β-PIXb (five independent experiments; one-way ANOVA, Tukey–Kramer post-test; ***, $P < 0.001$). Data are normalized to Rac1-transfected cells, the value of which (1) is indicated by dotted line. Error bars indicate SEM. (d, left) Immunoblot of HEK293T cells expressing KCC2b and/or β-PIXb using anti-phospho-cofilin and anti-cofilin antibodies as well as anti-KCC2 and anti–β-PIX antibodies. Black lines separate different sets of samples on the continuous blot. (right) Quantification of phospho-cofilin to cofilin ratio normalized to the ratio in mock-transfected cells. The value of mock transfected cells (1) is indicated by a dotted line (five independent experiments; one-way ANOVA, Tukey–Kramer post-test; ***, $P < 0.001$). Error bars indicate SEM.

main), a β-PIX mutant incapable of GEF activity (Saneyoshi et al., 2008). Notably, neurons overexpressing KCC2b-C568A alone or in combination with β-PIXb or β-PIXb–DHm, exhibited comparable FRET signal levels, similar to β-PIXb–DHm–transfected neurons, ∼60% of control. It is likely that such level of FRET occurs when endogenous β-PIX is strongly inhibited, as overexpression of β-PIXb–DHm represses endogenous β-PIX in a dominant-negative manner (Saneyoshi et al., 2008). Thus, KCC2 is able to strongly inhibit β-PIX GEF activity, similarly to the dominant-negative β-PIX mutant DHm. In summary, the results of FRET analysis let us conclude that KCC2 controls Rac1 activation through regulation of β-PIX GEF activity in neurons.

KCC2 and β-PIX are colocalized in dendrites and dendritic spines of neurons

We performed double immunostaining of mouse brain sections with the anti-KCC2 and anti–β-PIX antibody to study whether endogenous KCC2 and β-PIX are colocalized in vivo. To be able to visualize dendrites and spines, we used trans-

Published June 8, 2015

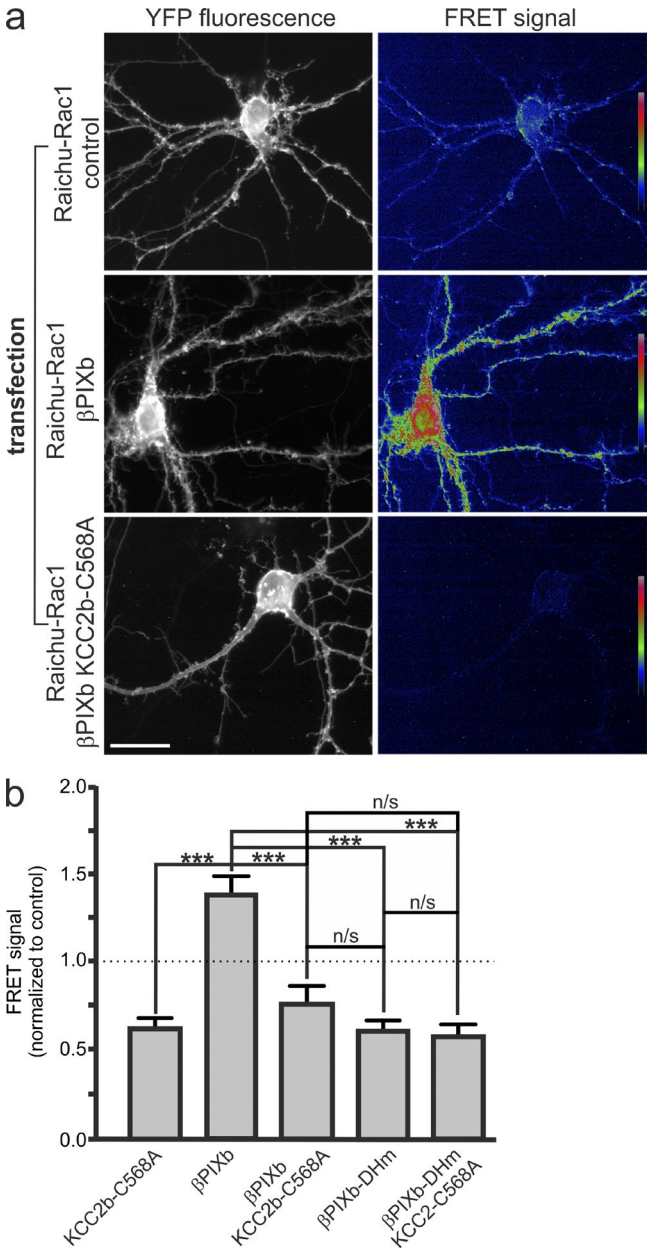

Figure 4. **KCC2 inhibits β-PIX–induced Rac1 activation in neurons.** (a) Representative image of cultured neurons expressing FRET sensor Raichu-Rac1 as well as β-PIXb alone or with KCC2b mutant C568A. (left) Fluorescence of YFP channel. (right) Corresponding images depicting FRET signal. Rac1 activation in FRET images is highlighted by pseudocolor. Bar, 20 µm. (b) Quantification of Raichu-Rac1 FRET signal in neurons (27–67 neurons per condition; Kruskal–Wallis test, Dunn's post-test; ***, $P < 0.001$; not significant [n/s], $P > 0.05$). The values were normalized to that of cells expressing Raichu-Rac1 only (1, indicated by a dotted line). Error bars indicate SEM.

genic mice expressing YFP under the Thy1 promoter, where YFP is expressed in a sparse subpopulation of neurons (Feng et al., 2000). Fig. 5 a shows an example of such immunostaining. We performed colocalization analysis on 3D confocal image stacks using Imaris 6 software (Bitplane). The result of this analysis is highlighted in white in the rightmost image of Fig. 5 a. Indeed, colocalization of KCC2 and β-PIX signals was observed in spines as well as on dendritic shafts and in neuronal soma. Pearson coefficient of colocalization was ∼0.58. Because in Thy1-YFP mice brain only few neurons express YFP, we observed KCC2, β-PIX, and colocalization signals that are outside the YFP-expressing dendrite and that belong to surrounding neurons not expressing YFP.

To analyze in more details KCC2 and β-PIX expression in dendritic spines with different morphology, we used a set of immunostainings of DIV 21 dissociated hippocampal cultures (Fig. 5 b). We segregated dendritic spines into four groups: mushroom, stubby, thin, and filopodia, based on the spine length and the diameter of the spine head (Materials and methods; see Table 1). Interestingly, both KCC2 and β-PIX were expressed at higher levels in mushroom spines and at lower levels in filopodia (Fig. 5 c). Because spine head diameter correlates with synaptic strength (Takumi et al., 1999), immunostaining data indicate that KCC2 and β-PIX expression is higher in mature spines with active synapses.

KCC2 controls glutamatergic synaptogenesis through regulation of β-PIX activity

Actin dynamics play an indispensable role in synaptogenesis (Ethell and Pasquale, 2005). KCC2-deficient neurons are known to form less functional synapses (Li et al., 2007; Gauvain et al., 2011), possibly as a consequence of impaired actin regulation (Fig. 1 b). Similarly to KCC2, β-PIX is known to control synapse formation (Zhang et al., 2005; Saneyoshi et al., 2008). The activity of β-PIX is stimulated by phosphorylation of serine 516 by CaMKI. Substitution of β-PIXb serine 516 to alanine produces a dominant-negative form of β-PIX (β-PIX–S516A) that cannot be phosphorylated at this residue. Expression of β-PIX–S516A in neurons decreases synapse number, similarly to β-PIX knockdown by siRNA (Saneyoshi et al., 2008).

Because KCC2 inhibits GEF activity of β-PIX toward Rac1 (Fig. 4 b), diminished KCC2 expression should result in increased β-PIX activity. We took advantage of RNA interference approach (Pellegrino et al., 2011) to suppress endogenous KCC2 expression in DIV 13–14 dissociated hippocampal neurons. This approach let us minimize accumulated side effects of KCC2 KOs related to the long-term absence of KCC2. We found that intensity of Raichu-Rac1 FRET signal in dendrites of neurons transfected with KCC2 shRNA was significantly higher than in neurons transfected with control (scrambled) shRNA (Fig. 6, a and b), indicating enhanced activity of GEFs toward Rac1. To assess whether this augmented FRET signal was specifically caused by increased β-PIX activity, we overexpressed β-PIX–S516A together with KCC2 shRNA. The effect of KCC2 deficiency on FRET signal was fully abolished by β-PIX–S516A (Fig. 6 b). These data further confirm functional interaction between endogenous KCC2 and β-PIX in neurons.

To address the relationship between KCC2 and β-PIX during synaptogenesis, we analyzed spines and glutamatergic synapses in DIV 13–14 dissociated hippocampal cultures expressing KCC2 shRNA. We visualized synapses by immunostaining for the presynaptic VGLUT1 (vesicular glutamate transporter-1) and the postsynaptic density protein PSD95 (Fig. 6 c). Synapses were identified as PSD95-positive clusters inside the transfected dendrite opposed by VGLUT1-positive presynaptic terminals. As expected, neurons transfected with KCC2 shRNA had ∼40% less spines and synapses than neurons transfected with scramble shRNA (Fig. 7 a).

Published June 8, 2015

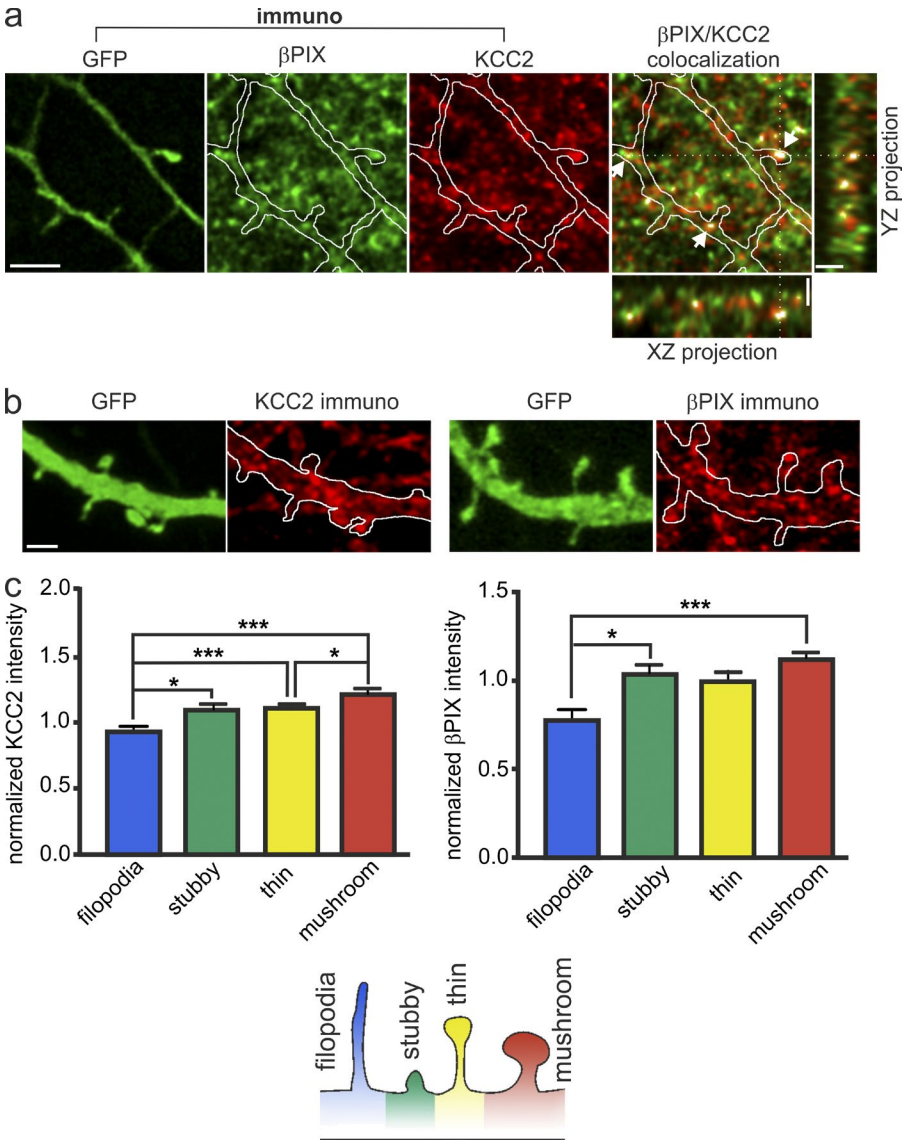

Figure 5. **KCC2 and β-PIX are colocalized in vivo.** (a) Representative immunostaining of endogenous β-PIX (green) and KCC2 (red) performed in hippocampus (pyramidal neuron in CA1 area) of an adult mouse expressing YFP under Thy1 promoter. Panels show a single confocal optical section (thickness of 0.21 µm) as well as XZ and YZ orthogonal projections of the confocal stack (30 optical sections, thickness of 6.3 µm). Projections are made along the white dashed lines. The rightmost image and orthogonal projections also show the result of 3D colocalization analysis, superimposed in white color. Pearson coefficient of colocalization is 0.58 ± 0.04; $n = 3$. Arrows highlight three colocalization spots detected by the analysis inside the YFP-expressing dendrite in the depicted confocal section. One spot is located inside a dendritic spine, and two are in dendritic shafts. The lines for orthogonal projections are selected so that the spot in the spine is visible in both XZ and YZ projections. Bars, 3 µm. (b) Immunostaining of GFP-transfected cultured hippocampal neurons with anti-KCC2 (left) or anti–β-PIX (right) antibodies. Bar, 2 µm. (c, top) Graphs depicting the distribution of KCC2 (left) and β-PIX (right) in different spines when analyzed in cultured hippocampal neurons (KCC2: 195–350 spines per group; β-PIX: 39–130 spines per group; Kruskal–Wallis test, Dunn's post-test; *, $P < 0.05$; ***, $P < 0.001$). (bottom) Schematic representation of morphologies of filopodia and three types of dendritic spines. Error bars indicate SEM.

KCC2-deficient neurons also had increased inter-event interval of miniature excitatory postsynaptic currents (mEPSCs; Fig. 7 c), implying the reduction of the number of functional synapses. These results are in agreement with previous data (Li et al., 2007; Gauvain et al., 2011) and confirm that KCC2 regulates synaptogenesis.

To assess whether the effect of KCC2 on synapse formation involves β-PIX activity, we combined shRNA-mediated knockdown of KCC2 with expression of the dominant-negative β-PIXb–S516A. Neurons with suppressed β-PIX activity, i.e., transfected with β-PIXb–S516A in the presence of control (scrambled) shRNA, exhibited reduced number of spines and synapses (Fig. 7 a) as well as increased inter-event interval of mEPSCs (Fig. 7c). Notably, knockdown of KCC2 in the neurons with suppressed β-PIX activity produced no further changes.

We also analyzed dendritic spine head diameter and found that expression of KCC2 shRNA resulted in a significant increase in head size (Fig. 7 b). This effect was also abolished in the presence of β-PIXb–S516A. Thus, when β-PIX functionality is impaired by the dominant-negative mutant, ablation of KCC2 produces no effect on the number and morphology of spines as well as on the number of functional synapses. These results indicate that KCC2 regulates spine morphology and glutamatergic synaptogenesis in neurons through β-PIX.

KCC2 deficiency in neurons decreases protrusive motility of dendritic spines

Dendritic spines exhibit rapid motility that depends on actin cytoskeleton dynamics (Bonhoeffer and Yuste, 2002). Protrusive motility of spines consists of fast elongation and retraction. It is of major importance during synaptogenesis, and it is believed to promote formation of the initial synaptic contact with an appropriate axon (Tashiro and Yuste, 2004).

Here, we analyzed the motility of dendritic spines in DIV 21 cultured hippocampal neurons, where KCC2 expression was suppressed by RNA interference during 4 d leading up to the experiment. We used live time-lapse confocal imaging to assess the motility. Upon KCC2 knockdown, protrusive motility of spines was reduced by 25% (Fig. 7 d). Reduced motility is in line with the impaired actin turnover in KCC2-deficient neurons and may account, at least partly, for the insufficient synaptogenesis found in KCC2-deficient neurons.

Published June 8, 2015

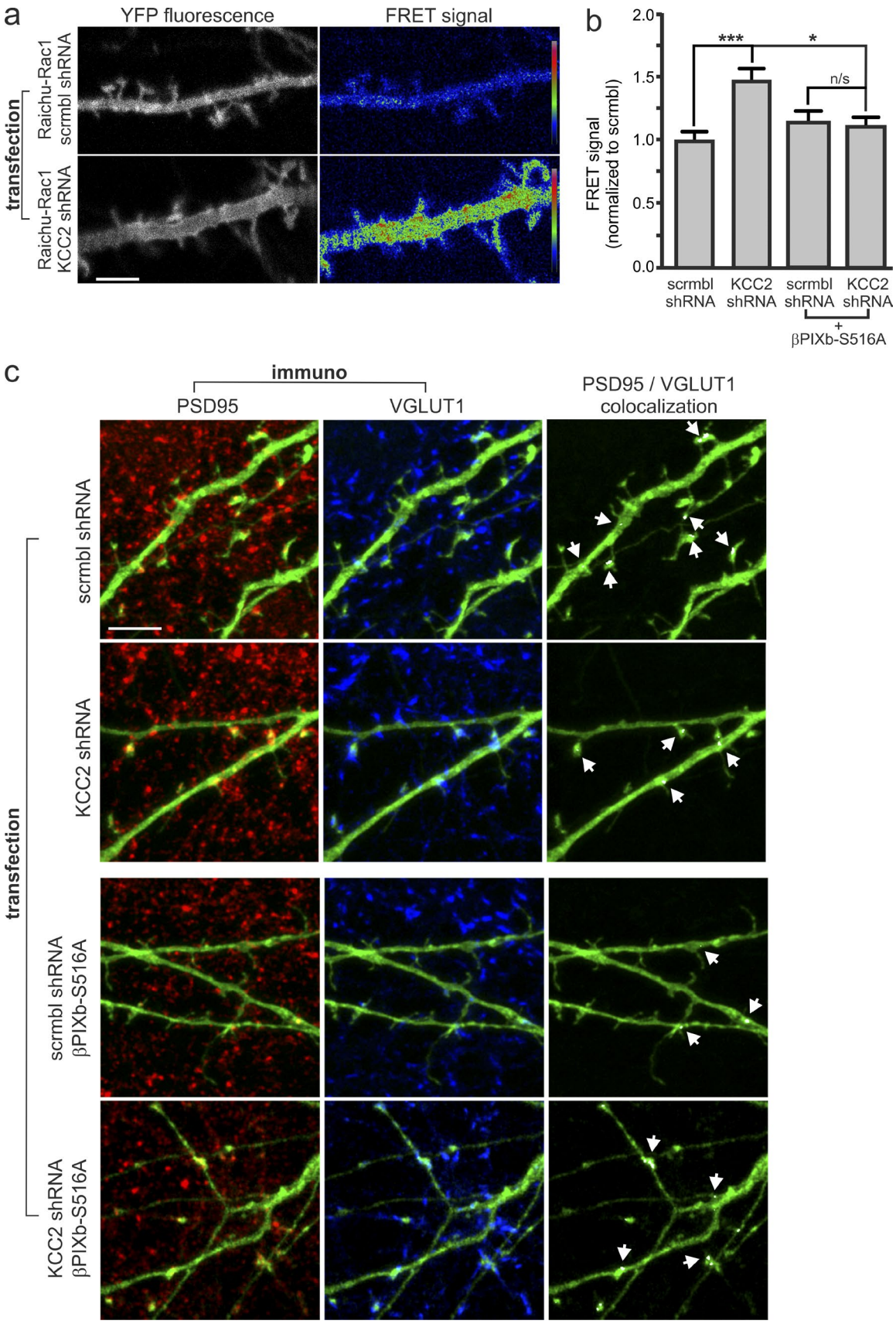

Figure 6. **Glutamatergic synapses in neurons with altered functional expression of KCC2 and β-PIX.** (a) Representative image of cultured neurons expressing FRET sensor Raichu-Rac1 as well as control shRNA (scrambled [scrmbl] shRNA) and KCC2 shRNA alone or in the presence of β-PIXb mutant S516A. (left) Fluorescence of YFP channel. (right) Corresponding images depicting FRET signal. Rac1 activation in FRET images is highlighted by pseudo

Published June 8, 2015

Discussion

In the present work, we report a novel pathway for the direct regulation of actin cytoskeleton dynamics by KCC2. In particular, we show that KCC2 interacts with β-PIXb and inhibits β-PIX–induced activation of the small GTPase Rac1. Our data provide evidence that KCC2 regulates formation of glutamatergic synapses through control of β-PIX activity.

We have previously found that KCC2-deficient neurons fail to develop mature dendritic spines (Li et al., 2007). Now, we demonstrate that KCC2 deficiency results in augmented stability of actin filaments, most likely as a result of increased phosphorylation of the actin depolymerizing factor cofilin-1. Our data corroborate previous studies showing that premature or ectopic expression of KCC2 affects the structure of the actin cytoskeleton in developing neurons (Horn et al., 2010) and in cancer cells (Wei et al., 2011). Although we focused our study on neuronal spines and synapses, KCC2 could also be involved in actin regulation in other systems.

We show that regulation of actin filament stability by KCC2 is independent of its activity as an ion transporter. This finding further confirms the capacity of KCC2 to control intracellular processes through interaction with other proteins (Chamma et al., 2012; Blaesse and Schmidt, 2015). Several proteins have been reported to interact with KCC2 (Ikeda et al., 2004; Inoue et al., 2004; Ivakine et al., 2013; Mahadevan et al., 2014). Among them 4.1N, a FERM domain protein, was shown to mediate the role of KCC2 in morphogenesis of dendritic spines (Li et al., 2007) and could also be attributed to KCC2-mediated regulation of actin stability. However, there is no evident connection between 4.1N and regulation of cofilin-1 or actin dynamics in the literature. Furthermore, because in our experiments, the mutant KCC2-C568A restores impaired stability of actin filaments and phospho-cofilin levels, whereas a previous study has shown that it does not interact with 4.1N (Horn et al., 2010), our data indicate a novel, 4.1N-independent, pathway through which KCC2 regulates actin turnover.

An important novel finding of this study is that KCC2 interacts with β-PIXb (Fig. 3 and Fig. S2 a), a GEF for small GTPases Rac1 and Cdc42 (Manser et al., 1998). β-PIX, through activation of Rac1, forms part of the signaling cascade controlling cofilin-1 phosphorylation (Saneyoshi et al., 2008; Mizuno, 2013); thus, the interaction with β-PIX may explain KCC2-mediated alterations in cofilin phosphorylation levels. Indeed, by using two independent Rac-1 activation assays, we found that KCC2 inhibits β-PIX GEF activity toward Rac1 both in HEK293T cells and in neurons (Fig. 3 c, Fig. 4, and Fig. 6, a and b). Accordingly, coexpression of KCC2b and β-PIXb resulted in a significant reduction of cofilin-1 phosphorylation in HEK293T cells (Fig. 3 d). Mutation of the proline-rich motif in KCC2 C terminus does not disrupt its interaction with β-PIXb (Fig. S2 b); thus, the site of interaction remains to be identified.

How does KCC2 affect endogenous β-PIX GEF activity? One possibility is that KCC2 regulates β-PIX synaptic localization, which is crucial for Rac1 activation (ten Klooster et al., 2006), possibly by disrupting β-PIX interaction with scaffold proteins GIT1 and Shank (Park et al., 2003; Zhang et al., 2003). However, our data do not support this model because we do not observe a change of β-PIX distribution in spines and shafts of KCC2 KO neurons (Fig. S3). Alternatively, KCC2 might affect the ability of β-PIX to form part of its signaling complex (Pertz, 2010), or it might alter the phosphorylation state of β-PIX (Saneyoshi et al., 2008). Identifying and mutating the KCC2–β-PIX interaction site remain a scope for our further research and would help to decipher the regulatory mechanisms acting in this novel pathway.

Our data indicate that endogenous KCC2 and β-PIX are coexpressed in mature spines, where they regulate Rac1 activity and cofilin-1 phosphorylation status, whereas both Rac1 and cofilin-1 are known to play a pivotal role in spine morphogenesis. It is becoming more evident that dynamic modulation of proteins involved in actin regulation is required for spine development and plasticity (Hotulainen and Hoogenraad, 2010; Pertz, 2010). For example, knockdown of cofilin-1 by siRNA and overexpression of constitutively active cofilin-1 induces similar phenotype in developing neurons: long filopodia-like structures (Hotulainen et al., 2009; Shi et al., 2009). Similarly, both long-term increase and decrease of Rac1 activity leads to reduced number of normal spines and synapses (Nakayama et al., 2000; Zhang et al., 2003). Thus, the shift in actin turnover balance in either direction results in disrupted spine and synapse development.

With this as background, we suggest that KCC2 expression in dendritic spines adjusts the appropriate ratio between active and inactive forms of β-PIX, providing an important mechanism for balanced activation of Rac1 and cofilin-1 and subsequent modulation of cytoskeleton structure. A simplified model of this regulation is schematically depicted in Fig. 8. The dynamic nature of the interaction between KCC2 and β-PIX implies that it is tightly regulated in time and space according to intracellular and/or extracellular cues. Although our study does not provide data on the mechanisms that might affect efficiency of the interaction, we can speculate that among such regulatory factors may be interactions of KCC2 and/or β-PIX with other proteins, including those known to mediate the role of KCC2 in synaptogenesis, such as 4.1N, Neto2, and kainate receptors (Li et al., 2007; Ivakine et al., 2013; Mahadevan et al., 2014).

According to this model, KCC2 deficiency leads to overactivation of β-PIX and Rac1. In this context it is remarkable that overactivation of Rac1 caused by overexpression of β-PIX (Zhang et al., 2003, 2005), or constitutively active Rac1 (Nakayama et al., 2000; Zhang et al., 2003) results in formation of aberrant dendritic protrusions and reduction of normal spines and synapses, the phenotype characteristic of KCC2-deficient neurons (Li et al., 2007; Gauvain et al., 2011). Apart from experimental manipulations, KCC2 deficiency in spines may be caused by pathophysiological conditions, such as epilepsy or brain trauma, that are known to cause a robust down-regulation of KCC2 (Medina et al., 2014). In the developing brain, this would lead to spine malformation and alteration of synaptogen-

color. Bar, 8 µm. (b) Quantification of Raichu-Rac1 FRET signal in dendrites (44–57 dendrites per condition; Kruskal–Wallis test, Dunn's post-test; ***, $P < 0.001$; *, $P < 0.05$; not significant [n/s], $P > 0.05$). Error bars indicate SEM. (c) Immunostaining of hippocampal neurons overexpressing control shRNA (scrambled shRNA) and KCC2 shRNA alone or in the presence of β-PIXb mutant S516A. GFP was coexpressed with other constructs to visualize transfected neurons. Antibodies against VGLUT1 (blue) and PSD95 (red) were used to identify pre- and postsynaptic sites, respectively. The colocalization of PSD95 and VGLUT1 (shown in white and highlighted with arrows at the rightmost column) was used to measure the density of glutamatergic synapses. Bar, 5 µm.

Published June 8, 2015

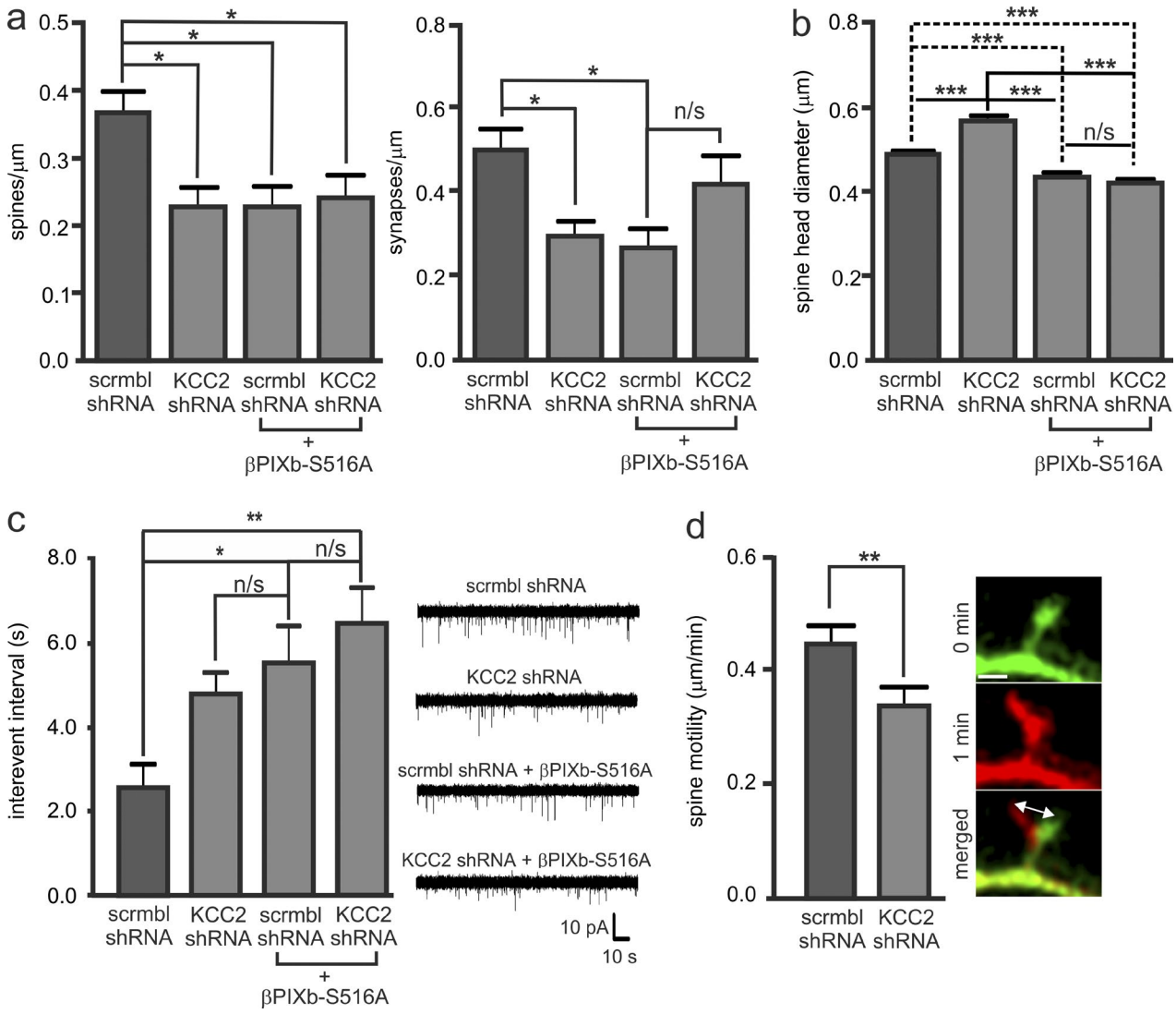

Figure 7. **KCC2 and β-PIX regulate synapse formation.** (a) Quantification of the density of spines (left) and glutamatergic synapses (right; spines: 10–14 dendrites per condition; synapses: 12–26 dendrites per condition; Kruskal–Wallis test, Dunn's post-test; *, $P < 0.05$; not significant [n/s], $P > 0.05$). Error bars indicate SEM. (b) Quantification of spine head diameter (314–504 spines per condition; Kruskal–Wallis test, Dunn's post-test; ***, $P < 0.001$; not significant [n/s], $P > 0.05$). (c, right) Depictive traces of the electrophysiological recordings of mEPSCs in cultured hippocampal cells overexpressing control shRNA (scrmbl shRNA) or KCC2 shRNA alone or in the presence of β-PIXb mutant S516A. (left) Quantification of the mEPSCs inter-event intervals (6–12 neurons per condition; one-way ANOVA, Tukey–Kramer post-test; *, $P < 0.05$; **, $P < 0.01$; not significant [n/s], $P > 0.05$). Error bars indicate SEM. (d, right) Illustrative time-lapse images of a spine showing lateral protrusive motility. The double-pointed arrow highlights the distance traveled by the spine during 1 min. Bar, 2 µm. (left) Quantification of protrusive motility in hippocampal cells overexpressing KCC2 shRNA or control shRNA (scrambled shRNA: 22 spines; KCC2 shRNA: 24 spines; Mann–Whitney test, $P = 0.0075$). Error bars indicate SEM.

esis that might further contribute to the long-term consequences of pathological insults early in life.

To conclude, in this study, we describe a novel role for KCC2 in the regulation of the actin cytoskeleton in dendritic spines of neurons. This pathway may provide important modulation of critical steps in the formation and maturation of glutamatergic transmission, such as the rate of first contact between pre- and postsynaptic sites and the stabilization of mature dendritic spines.

Materials and methods

Cell culture

All animal experiments were approved by the local ethics committee for animal research at the University of Helsinki. Standard dissociated hippocampal and cortical cultures were prepared from embryonic day 17 (E17) mice and cultured for up to 3 wk in vitro. We used the protocol described in Banker and Goslin (1998), with minor modifications. In brief, a pregnant mouse was anaesthetized in a CO_2 chamber and killed by cervical dislocation, embryos were removed, and hippocampi were dissected. Cells were dissociated by enzymatic treatment (0.25% trypsin for 15 min at 37°C) and plated on poly-DL-ornithine–coated cover glasses (10^5 cells/cm^2) in Neurobasal medium containing B27 supplement and 0.5 mM L-glutamine (Gibco/Life Technologies). Before plating, the medium was preincubated on astroglial culture for 24 h. Neuronal cultures were fed once a week by changing half of the medium. Astroglial cultures were prepared according to Banker and Goslin (1998). In brief, dissociated hippocampal cells were prepared as described above and plated on uncoated plastic surface. Since neurons need specific coating for attachment, the resulting culture did not

Published June 8, 2015

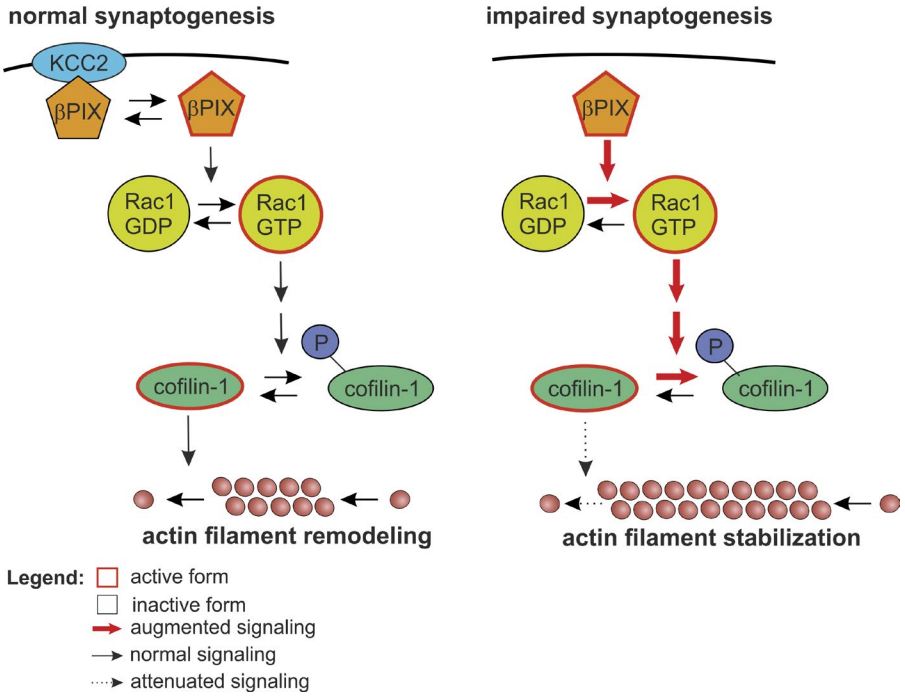

Figure 8. **A model of KCC2-mediated regulation of actin dynamics.** According to this model, in spines, KCC2 regulates the balance between active and inactive β-PIX that is crucial for dynamic actin remodeling. In the case of KCC2 deficiency, β-PIX and Rac1 are overactivated, whereas cofilin is mostly in its phosphorylated form, which leads to freezing of actin turnover. P, phosphorylation.

contain neurons. This method, together with the use of standard medium (DMEM [Gibco/Life Technologies] supplemented with 10% of fetal bovine serum, 100 U/ml penicillin, and 100 µg/ml streptomycin), favors glial survival over neurons. Every 4 wk, glia cells were subcultured to a new dish to maintain 30–70% confluence.

HEK293T cells were cultured in DMEM supplemented with 10% fetal bovine serum, 100 U/ml penicillin, and 100 µg/ml streptomycin. The number of cell passages was limited to 20 after thaw.

Western blotting

Neuronal or HEK293T cultures were rinsed in PBS, scraped, and homogenized in ice-cold radioimmunoprecipitation lysis buffer (150 mM NaCl, 1% Triton X-100, 0.5% deoxycholate, 0.1% SDS, and 50 mM Tris-HCl, pH 8.0) with protease inhibitor cocktail (cOmplete; Roche) and phosphatase-inhibitor cocktail (PhosSTOP; Roche). Protein concentrations were determined using DC Protein Assay kit (Bio-Rad Laboratories, Inc.). Samples were loaded in Laemmli sample buffer (63 mM Tris-HCl pH 7, 2% SDS, 20% glycerol, 5% β-mercaptoethanol, and bromophenol blue), separated using SDS-PAGE, and transferred to nitrocellulose membrane (Hybond ECL; GE Healthcare). Blots were probed with the appropriate primary antibodies (see Antibodies) and HRP-conjugated donkey anti–rabbit (GE Healthcare) or goat anti–chicken IgY (Abcam) antibodies and then developed with ECL Plus (GE Healthcare) and visualized with LAS-3000 (Fujifilm). Band densities were analyzed with AIDA imaging software (Raytest).

Cell transfection

1 d before transfection, half of the medium of cultured neurons was changed to fresh glia-conditioned medium. For neurons older than 10 DIV, 1 h before transfection culture medium was substituted by 10 mM $MgCl_2$ in Neurobasal medium. Neurons were transfected with 0.5 µg of plasmid DNA per 1.6-cm^2 well using Lipofectamine 2000 (Invitrogen/Life Technologies) according to the manufacturer's protocol. Culture medium was returned to the cells 4–6 h after transfection. Cultured HEK293T cells were transfected using jetPEI reagent (Polyplus Transfection) or Calcium Phosphate Transfection kit (Invitrogen/Life Technologies) according to provider's instructions.

Plasmids

Rat KCC2b cDNA (donated by J. Payne, University of California, Davis, Davis, CA) was cloned into the pcDNA3.1 expression vector (cytomegalovirus promoter) and verified by DNA sequencing. Rat KCC2-C568A and KCC2-Y1087D were generated using the site-directed mutagenesis kit (QuikChange; Agilent Technologies) and verified by DNA sequencing. The mutations were made on the rat KCC2b sequence subcloned into the home-modified Takara Bio Inc. backbone vector including an ubiquitin promoter. KCC2 shRNA (5′-GACATTGGTAATGGAACAACG-3′) and scramble shRNA (5′-GATGAACCTGATGACGTTC-3′) were described previously (Pellegrino et al., 2011). KCC2-CTD was generated by subcloning CTD fragment (amino acids 845–1,116) of mouse KCC2 sequence into modified pRK5-myc vector using XhoI and HindIII restriction enzymes. The open reading frame of rat β-PIXb was cloned in pDest27 using the Gateway technology (Invitrogen). To generate the KCC2-CTD PP→QA mutant, the KCC2 fragment (813–1,116 aa) with P1077Q and P1078A mutations and Kozak sequence was produced by a gene synthesis service (Invitrogen) and cloned into the pcDNA3 vector using BamHI and HindIII restriction sites. Human β-PIXb–S516A and β-PIXb–DHm in pCAGGS were provided by G. Wayman and D. Guimond (Washington State University, Pullman, WA; Saneyoshi et al., 2008). In brief, cDNA for human β-PIX (GenBank accession no. BC050521) was obtained from GE Healthcare and cloned into pCAGGS (CAG promoter). Site-directed mutagenesis of β-PIX (S516A and DHm [L238R, L239S]) was performed using a mutagenesis kit (QuikChange; Agilent Technologies).

GFP–β-actin was obtained from M.K. Vartiainen (Institute of Biotechnology, University of Helsinki, Helsinki, Finland; Dopie et al., 2012). In brief, human β-actin was subcloned into pEGFP-C1 (Takara Bio Inc.) using KpnI and HindIII restriction sites. pRK5-myc-Rac1-wt was a deposit in a database by the laboratory of G. Bokoch (The Scripps Research Institute, San Diego, CA; Addgene plasmid 12985). Concisely, human Rac1 (GenBank accession no. AF498964) was cloned into pRK5-myc vector (cytomegalovirus promoter) by cutting at BamHI and EcoRI restriction sites (sites are maintained intact). Raichu-Rac1 was a gift from M. Matsuda (Itoh et al., 2002). In short, Raichu-Rac consists of YFP (aa 1–239), a spacer (Leu-Asp), Cdc42/

Published June 8, 2015

Rac interactive binding motif of PAK1 (aa 68–150), a spacer (Ser-Gly-Gly-Thr-Gly-Gly-Gly-Gly-Thr), Rac1 (aa 1–176), a spacer (Gly-Gly-Arg), CFP (aa 1–237), a spacer (Gly-Arg-Ser-Arg), and the CAAX box of Ki-Ras (aa 169–188) cloned into pCAGGS (CAG promoter).

Antibodies

Rabbit anti-phospho-cofilin antibodies (serine 3) were purchased from Santa Cruz Biotechnology, Inc. Rabbit anti–cofilin-1 (recombinant mouse full-length cofilin-1) antibodies were provided by M.K. Vartiainen (Hotulainen et al., 2005). Guinea pig anti-VGLUT1 antibodies, monoclonal mouse anti-PSD95, and polyclonal rabbit anti–β-PIX (SH3 domain) were purchased from EMD Millipore. Rabbit polyclonal antibodies anti-PAK1/2/3 were acquired from Cell Signaling Technology. Mouse monoclonal antibodies against GFP were purchased from Roche. The chicken anti-KCC2b antibodies (Markkanen et al., 2014) as well as the KCC2 pan-antibodies (Ludwig et al., 2003) were produced and purified by Innovagen AB.

Immunocytochemistry

Neurons were fixed with 4% paraformaldehyde in PBS at RT and permeabilized with 0.1% Triton X-100. Cells were blocked with 10% goat/donkey serum and 0.1% Triton X-100 in PBS at RT and then incubated at 4°C overnight in 5% goat/donkey serum containing the appropriate primary antibodies. Species-specific goat anti–guinea pig Alexa Fluor 568 (Invitrogen/Life Technologies) and donkey anti–mouse or anti–rabbit Cy5 (Jackson ImmunoResearch Laboratories, Inc.) secondary antibodies were used. Cover glasses were mounted in ProLong Gold mounting media (Life Technologies).

Immunohistochemistry

Paraffin coronal sections of the hippocampi of an adult mouse (postnatal day 30) expressing YFP under Thy1 promoter (B6.Cg-Tg(Thy1-YFP-PH)2Jrs/J mice, stock number 003782; The Jackson Laboratory) were costained for KCC2b and β-PIX as described previously (Ludwig et al., 2003) with modifications. Concisely, deparaffinized sections were washed in SDS solution, and masked epitopes were retrieved subsequently by heating the samples in a microwave oven for 12 min at 700 W in a solution containing 1 mM EDTA, 1 mM sodium citrate, and 2 mM Tris-HCl, pH 8.5. To avoid desiccation of the samples during the microwave treatment, more solution was added frequently. Cooled down samples were washed with TBST, blocked with 5% BSA in TBST, and incubated with primary antibodies in 2% BSA and 0.2% Triton X-100 in TBST overnight at 4°C. To reveal YFP, mouse anti-GFP antibodies were applied to the incubation solution. Species-specific secondary antibodies donkey anti–mouse Alexa Fluor 488, goat anti–chicken Alexa Fluor 568 (Invitrogen/Life Technologies), and donkey anti–rabbit Cy5 (Jackson ImmunoResearch Laboratories, Inc.) were used in 2% BSA and 0.2% Triton X-100 in TBST (TBS with Tween). Cover glasses were mounted in ProLong Gold mounting media (Life Technologies).

Yeast two-hybrid

The C-terminal segment of KCC1 (amino acids 643–1,085; GenBank accession no. NM_019229), KCC2 (amino acids 644–1,116; GenBank accession no. U55816), KCC3a (amino acids 677–1,099 GenBank accession no. AF211854), KCC4 (amino acids 891–1,340; GenBank accession no. NM_001013144), and NKCC1 (amino acids 725–1,203; GenBank accession no. AF051561) were cloned into the vector pLexN as baits and β-PIXb (amino acids 375–705; GenBank accession no. AY996221) into pVp16 as prey. Thereafter, L40 yeast strain was transformed with a corresponding pair of bait and prey plasmids, and cells were grown overnight. Then, 2 ml of the overnight grown culture were transferred to new medium and incubated for 5 h at 30°C. Subsequently, OD_{600} was determined, and cells were lysed via freeze–thaw cycles in liquid nitrogen. Color reaction was initiated by the addition of 700 µl Z buffer (60 mM Na_2HPO_4, NaH_2PO_4, 10 mM KCl, and 1 mM $MgSO_4$) with 160 µl *o*-nitrophenyl-β-D-galactoside solution (solubilized in Z buffer) to the samples. The samples were incubated for 1 h at 37°C. The reaction was stopped by the addition of 400 µl of 1 M Na_2CO_3. After centrifugation, the absorption values of the samples were measured at 420 nm. Finally, the β-galactosidase units were calculated according to Miller (1972).

Immunoprecipitation analysis of the brain tissue

All preparations and centrifugations were performed at 4°C. All solutions contained cOmplete protease inhibitor cocktail and phosphatase-inhibitor cocktail (PhosSTOP). Native membrane fractions and immunoprecipitations were prepared similarly to previously described (Mahadevan et al., 2014) with slight modifications. One adult male NMRI mouse brain (P40–60) was manually homogenized in 5 ml PBS using a glass Teflon homogenizer. The homogenate was centrifuged at 900 *g* for 10 min, and the pellet was resuspended in 5 ml ice-cold lysis buffer (50 mM Tris-HCl, pH 7.5, and 1 mM EDTA) by pipetting. The homogenate was subsequently centrifuged for 30 min at 25,000 *g*. The native membrane fractions were recomposed in 4× mass/volume solubilization buffer (50 mM Tris-HCl, pH 7.5, 50 mM NaCl, 0.05 mM EDTA, and 1.5% C12E9). The sample was let to solubilize for 2 h on a rotating wheel, followed by a centrifugation at 25,000 *g* for 1 h. Immunocomplexes of the membrane fractions were attained by incubation of 4–5 mg of membrane fraction homogenate with anti–β-PIX antibodies (EMD Millipore) for 3 h in a rotating wheel. Subsequently, the immunocomplexes were precipitated by incubation with 25 µl Gamma-Bind G–Sepharose beads (GE Healthcare) for 1 h with rotation. Next, the beads were washed twice with solubilization buffer containing detergent (1.5% C12E9) and once with solubilization buffer without detergent. Elution of proteins was performed by incubation of the precipitated beads in 50 µl Laemmli sample buffer (63 mM Tris-HCl, pH 7, 2% SDS, 20% glycerol, 5% β-mercaptoethanol, and bromophenol blue) at 95°C for 5 min and then analyzed by Western blotting with antibodies against KCC2b, β-PIX, PSD95, and PAK1/2/3.

HEK293T cell immunoprecipitation analysis

The immunoprecipitation protocol was performed 40 h after transfection. Cells were washed twice with cold PBS and lysed in cold TNE buffer (1% Nonidet P-40, 140 mM NaCl, 5 mM EDTA, and 50 mM Tris-HCl, pH 8.0) supplemented with cOmplete protease inhibitor cocktail and phosphatase inhibitor cocktail (PhosSTOP) on ice for 15–20 min. The lysate was collected using a cell scraper and centrifuged to remove particulate matter. Cell lysate containing ∼1 mg of total protein was precleared for 1 h with G-Sepharose previously blocked in 5% milk-PBS and 0.1% Tween 20. Next, 3–5 µg polyclonal antibodies against β-PIX or KCC2b was added and incubated overnight. The immune complexes were precipitated by 2–4-h incubation with blocked G-Sepharose. The beads were washed several times with TNE buffer and once with PBS. The immune complexes were eluted by heating at 95° for 5 min in SDS sample buffer (1% SDS, 100 mM DTT, and 50 mM Tris-HCl, pH 7.5) and analyzed by Western blotting with antibodies against KCC2 and β-PIX.

Rac1 activation assay

Rac1 activity was measured using a Rac1 G-LISA colorimetric-based biochemical assay kit (Cytoskeleton, Inc.), according to manufacturer's instructions. In brief, HEK293T cells expressing respective constructs were serum-starved overnight. Cells were lysed and snap frozen in liquid nitrogen. After fast thawing, binding buffer was added to the

Published June 8, 2015

Table 1. **Dendritic spine classification parameters**

Spine type/parameter	Head	Length	Width/length ratio
		µm	
Filopodia	No	>1.2	Not applicable
Stubby	No/Yes	<1.2	If the head is present, <0.5; if no head, not applicable
Thin	Yes	>1.2	<0.5
Mushroom	Yes	Not applicable	>0.5

cell lysate and subsequently incubated on a Rac1-GTP affinity plate coated with Rac1-GTP–binding protein. The plate was placed on an orbital plate shaker at 300 rpm for 30 min. Cell lysis and incubations were performed in a cold cabinet at 4°C. After washes, anti-Rac1 antibodies (1:500) were added to the wells. Then, the primary antibody was washed away, and the HRP-linked secondary antibodies (1:500) were added to the wells. Both primary and secondary antibodies were incubated on the orbital shaker at 300 rpm for 45 min at RT. Thereafter, the signal was developed with HRP-detection reagents. The luminescence was measured by means of a multilabel plate reader spectrophotometer (VICTOR; PerkinElmer). Results are shown as relative luminescence units.

Microscope setups and image analysis

All confocal images (except FRET, which is described below) were acquired with a microscope (TCS SP5; Leica) equipped with the software LAS AF 1.82 and following lasers: optically pumped semiconductor laser 488 nm/270 mW, diode-pumped solid-state laser 561 nm/20 mW, and HeNe 633 nm/12 mW. For fixed samples, the glycerol immersion objective HCX Plan Apochromat 63×/1.3 NA GLYC CORR CS (glycerol correction; Leica) at RT was used. Live cell microscopy (FRAP and Motility analysis, see below) was carried with HCX Apochromat L 63×/0.90 NA water immersion objective. Neurons were maintained at 37°C and 5% CO_2 in a custom chamber (The Box; Life Imaging Services) in Neurobasal medium containing B27 supplement and 0.5 mM L-glutamine throughout the imaging session.

For quantification of phospho-cofilin in Fig. 2 b, fluorescent wide-field images were acquired with microscope (AxioImager.M1; Carl Zeiss) equipped with camera (AxioCam HR; Carl Zeiss) and AxioVision 4 software (Carl Zeiss). The hippocampal neurons were imaged with 40× objective EC Plan Neofluar/0.75/Ph2 at RT. The light-emitting diode system (Colibri; Carl Zeiss) with 470- and 555-nm modules was used, and the beam combiners were BC490, BC425 (for GFP), and BC565 (for Alexa Flour 568). The mean fluorescent density was measured in Image-Pro Plus 4 (Media Cybernetics) after subtraction of the background.

Colocalization analysis

The 3D (x, y, z) image stacks were blindly deconvoluted in AutoQuantX2 Deconvolution Software (Media Cybernetics) using the 3D deconvolution protocol and 10 iterations. Subsequently, the deconvoluted 3D images were analyzed in Imaris 6 software, and a representative image of the colocalization was created. For numerical colocalization analysis, the plugin JACoP (Bolte and Cordelières, 2006) in ImageJ (National Institutes of Health) was used. In brief, the suitable colocalization threshold was determined by Costes' automatic thresholding paradigm. Subsequently, the threshold was used to determine Pearson's coefficient of colocalization.

Spine characterization

The 3D (x, y, z) confocal images were blindly deconvoluted in AutoQuantX2 Deconvolution software (Media Cybernetics). The distribution of KCC2 and β-PIX in different spines was assessed in Imaris 6 software by building surfaces around the dendritic spines of hippocampal neurons expressing EGFP. Next, the intensity of KCC2 and β-PIX inside the spine surfaces was measured and normalized to the total intensity of KCC2 and β-PIX in the GFP-positive dendrite. Spines were classified according to the parameters summarized in Table 1.

Quantification of synapses

Blindly deconvoluted confocal stacks of neurons expressing GFP for visualization (deconvolution software AutoQuantX2) were analyzed in 3D (x, y, z) in Imaris 6 software. Synapses were detected by partial colocalization of the presynaptic marker anti-VGLUT1 antibody staining with postsynaptic anti-PSD95. A surface was rendered comprising of the GFP volume, and synaptic terminals were identified using the "spots near surface" function in the ImarisXT module. The number of colocalization spots situated at ≤0.4 µm from the rendered GFP surface was counted.

Quantification of spines and spine morphology

The deconvoluted confocal images of neurons acquired for the quantification of synapses were further analyzed in 3D using the software NeuronStudio (Wearne et al., 2005; Rodriguez et al., 2008). Automatic reconstruction of the dendritic shafts was followed by manual recognition and classification of spines by a trained researcher who was blind to the sample nature. The density of spines and spine head diameter were automatically calculated from the resulting model.

Motility analysis

Confocal images of neuronal cultures transfected with GFP were collected in time lapse every 60 s during 5 min and later analyzed in four dimensions (x, y, z, t) using Imaris 6 software. One stack of optical slices had physical size of 41 × 41 × 5.6 µm with the voxel size of 80 × 80 × 294 nm. 3D reconstructions were performed for each time point. To analyze the protrusive motility, spots were placed at the tip of every spine, and the total displacement of the dendritic spines was measured using the track length measurements in ImarisXT module.

FRAP

Fluorescence recovery of the actin-GFP intensity after photobleaching was measured as described previously (Koskinen et al., 2012) with slight modifications. In brief, FRAP was performed with a confocal microscope (TCS SP5; Leica) at 37°C and with 5% CO_2 in culture medium. To visualize dendritic spines, a 63×/0.90 NA dipping water objective and 6× digital zoom were used. The microscope was controlled by LAS AF 1.82 software, and the settings were as follows: format 256 × 256, speed 700 Hz (unidirectional), two-line averaging, and pinhole of 2.0 airy units. The frame of 41 × 41 µm, including the region of interest (the whole spine), was imaged five times before bleaching followed by photobleaching that was achieved with one scan (total bleach time = 1.5 s, total laser power = ∼2.2 mW) of the region of interest. Imaging of the area was resumed immediately after the photobleaching. A total of 66 frames were scanned during 152 s (26 frames

Published June 8, 2015

at 1 frame per 0.78 s and 20 frames at 1 frame per 2 s followed by 20 frames at 1 frame per 5 s). The intensity of the bleached area was normalized to a neighboring nonbleached dendritic area to diminish error caused by photobleaching during the monitoring period. The prebleach value was normalized to 1.0.

FRET

Dissociated hippocampal neurons were analyzed 2 d after transfection. Before imaging, neurons were preincubated in Neurobasal without B27 for 2 h at 37°C, 5% CO_2.

In the case of young neurons (DIV 7–9), fluorescence from Raichu-Rac1 was imaged and measured using an inverted microscope (IX71; Olympus) controlled by CellR software (Olympus) and equipped with oil immersion objective (U Apochromat/340 40×/1.35 NA) and digital camera (DBH1; Olympus). Cells were illuminated with a 150 W Xenon lamp (used at 40% of full power) through D436/20 (CFP) or HQ500/20 (YFP) excitation filters. Signal was collected using 480/40 (CFP) or 535/30 (YFP) emission filters. The exposure time was 1,000 ms. Before imaging, neurons were transferred into Hepes-buffered extracellular solution (124 mM NaCl, 3 mM KCl, 2 mM $CaCl_2$, 1.1 mM NaH_2PO_4, 2 mM $MgCl_2$, 10 mM Hepes, and 10 mM D-glucose, pH 7.4) and incubated 30 min before imaging in the same solution at RT.

In the case of the mature neurons (DIV 13–14), fluorescence from Raichu-Rac1 was imaged using a confocal microscope (LSM 710/Axio; Carl Zeiss) controlled by ZEN 2011 software (Carl Zeiss) and equipped with water immersion objective (63×/1.0 NA; Carl Zeiss), CO_2, and temperature control. The imaging was performed in culture medium at 5% CO_2 and 37°C. Dendrites of transfected neurons were illuminated with an argon laser (Lasos; Lasertechnik GmbH) at 458 nm (CFP and FRET) and 514 nm (YFP) using 0.5–10% of full laser power. Emission was collected at 461–519 nm (CFP) and 519–621 nm (FRET and YFP). The pinhole was fully opened. Scanning was performed in XY mode using 6× digital zoom that resulted in a pixel XY size of 68 × 68 nm.

For both young and mature neurons, FRET signal was calculated as reported elsewhere (van Rheenen et al., 2004) using ImageJ 1.48v software. In brief, after background subtraction, FRET image was generated using three images: M_{Donor} (CFP excitation and CFP emission filters), $M_{IndirectAcceptor}$ (CFP excitation and YFP emission filters), and $M_{DirectAcceptor}$ (YFP excitation and YFP emission filters), using the following equation: $FRET = (M_{IndirectAcceptor} - M_{Donor} \times \beta - M_{DirectAcceptor} \times (\gamma - \alpha\beta))/(1 - \beta\delta)$. Coefficients α, β, δ, and γ were obtained by independent control experiments analyzing cells expressing CFP or YFP as described in van Rheenen et al. (2004). Coefficients α, δ, and γ were determined in cells expressing only YFP (acceptor) and calculated according to equations: $\alpha = M_{Donor}/M_{DirectAcceptor}$; $\gamma = M_{IndirectAcceptor}/M_{DirectAcceptor}$; $\delta = M_{Donor}/M_{IndirectAcceptor}$. Coefficient β was determined in cells expressing only CFP (donor) and calculated according to the equation: $\beta = M_{IndirectAcceptor}/M_{Donor}$. After generation of FRET image, intensity of FRET signal was calculated using a mask obtained from a corresponding YFP image and covering neuronal cell bodies and dendrites.

Patch clamp recordings, data acquisition, and analysis

mEPSCs were recorded from cultured mouse hippocampal neurons (14–15 DIV) in a whole-cell voltage-clamp configuration at RT. The composition of the extracellular solution was 124 mM NaCl, 3 mM KCl, 2 mM $CaCl_2$, 1.1 mM NaH_2PO_4, 1.3 mM $MgCl_2$, 20 mM Hepes, and 10 mM D-glucose, pH 7.4. Neurons were in the extracellular solution maximally for 2 h. To eliminate synchronized action potential-induced spontaneous postsynaptic currents, all experiments were performed in the presence of 1 µM tetrodotoxin. mEPSCs of glutamatergic origin were isolated by extracellular application of 10 µM bicuculline methiodide. Miniature spontaneous events were completely and reversibly blocked by NBQX (2,3-dihydroxy-6-nitro-7-sulfamoyl-benzo[f]quinoxaline-2,3-dione); AMPA ([α-amino-3-hydroxy-5-methyl-4-isoxazolepropionic acid] receptor antagonist) and AP5 ([(2*R*)-amino-5-phosphonopentanoate]; NMDA [*N*-Methyl-D-aspartate] receptor antagonist). Patch pipettes were fabricated from borosilicate glass (GC-150F; Harvard Apparatus); and their resistance, when filled with intracellular solution (18 mM KCl, 111 mM potassium gluconate, 0.5 mM $CaCl_2$, 5 mM BAPTA ([1,2-bis(o-aminophenoxy)ethane-N,N,N′,N′-tetraacetic acid]; calcium-specific chelator), 2 mM Mg-ATP, 10 mM Hepes, 10 mM glucose, and 2 mM NaOH, pH 7.3), ranged from 6 to 8 MOhm. Membrane potential was clamped at −60 mV. Only cells with access resistance that did not exceed 20 MOhm were accepted for the analysis. Access and cell membrane resistance were regularly monitored by 100-ms-long 10-mV hyperpolarizing voltage pulses, and recordings were terminated if any of these resistances changed by 10% or more. A patch–clamp amplifier (EPC 9; HEKA) was used for voltage clamp and data acquisition. Data were acquired at a sampling rate of 2 kHz and then band-pass filtered (1 Hz–1 kHz). Synaptic events were detected and analyzed using Mini Analysis software (version 6; Synaptosoft, Inc.). After automatic screening (amplitude threshold set to 5 pA), events were approved manually according to their onset and decay. The inter-event interval for each individual cell was characterized by their median values.

Online supplemental material

Fig. S1 shows expression of KCC2 mutants C568A and Y1087D as well as expression of β-PIX and β-PIX–DHm in cultured neurons. Fig. S2 shows results of yeast two-hybrid assay of cation chloride cotransporters and β-PIXb, co-IP of β-PIXb with KCC2-CTD-PP→QA, and KCC2-C568A in HEK293T cells as well as immunoblot demonstrating equal expression of β-PIX alone or together with KCC2 in G-LISA assay. Fig. S3 shows the ratio of β-PIX density in spines/shafts of KCC2 KO hippocampal neurons. Online supplemental material is available at http://www.jcb.org/cgi/content/full/jcb.201411008/DC1.

Acknowledgements

We would like to thank Erja Huttu and Miika Palviainen for excellent technical assistance, Outi Nikkilä and Seija Lågas for isolation of hippocampal neurons, Gary Wayman and Damien Guimond for providing mutated β-PIX constructs, Gary Bokoch for depositing the WT Rac1 construct to Addgene, Nils Brose, George Rosenberger, and Kerstin Kutsche for help with the yeast two-hybrid screen, Perrine Friedel for help in creation of KCC2b-C568A and KCC2b-Y1087D mutants, Maria K. Vartiainen for providing the cofilin-1 antibody and GFP–β-actin construct, Michiyuki Matsuda for sharing Raichu-Rac1 FRET sensor, Kari-Pekka Skarp, Pavel Uvarov, Johan Peränen, Kari Keinänen, and Pekka Lappalainen for useful discussions, Vivek Mahadevan for helpful tips on the co-IP assays, and the staff at the Light Microscopy Unit (Institute of Biotechnology, Helsinki) for maintenance of the unit and technical assistance.

This work was supported by grants from the Academy of Finland (SA 259799 to C. Rivera; SA250742 to A. Ludwig), the Sigrid Juselius Foundation (to C. Rivera), University of Helsinki, University of Aix-Marseille, and Agence Nationale de la Recherche (ANR-13-BSU4-0012-01 to C. Rivera), the Integrative Life Sciences Doctoral Program (to O. Llano), and the Deutsche Forschungsgemeinschaft grant (no. 428/4-2 to H.G. Nothwang). C. Rivera is a member of the Finnish Center of Excellence in Molecular and Integrative Neuroscience.

The authors declare no competing financial interests.

Submitted: 4 November 2014
Accepted: 27 April 2015

References

Banker, G., and K. Goslin. 1998. Culturing Nerve Cells. Second edition. The MIT press, Cambridge, MA. 666 pp.

Blaesse, P., and T. Schmidt. 2015. K-Cl cotransporter KCC2—a moonlighting protein in excitatory and inhibitory synapse development and function. *Pflugers Arch.* 467:615–624. http://dx.doi.org/10.1007/s00424-014-1547-6

Bokoch, G.M. 2003. Biology of the p21-activated kinases. *Annu. Rev. Biochem.* 72:743–781. http://dx.doi.org/10.1146/annurev.biochem.72.121801.161742

Bolte, S., and F.P. Cordelières. 2006. A guided tour into subcellular colocalization analysis in light microscopy. *J. Microsc.* 224:213–232. http://dx.doi.org/10.1111/j.1365-2818.2006.01706.x

Bonhoeffer, T., and R. Yuste. 2002. Spine motility. Phenomenology, mechanisms, and function. *Neuron.* 35:1019–1027. http://dx.doi.org/10.1016/S0896-6273(02)00906-6

Calabrese, B., M.S. Wilson, and S. Halpain. 2006. Development and regulation of dendritic spine synapses. *Physiology (Bethesda).* 21:38–47. http://dx.doi.org/10.1152/physiol.00042.2005

Chamma, I., Q. Chevy, J.C. Poncer, and S. Lévi. 2012. Role of the neuronal K-Cl co-transporter KCC2 in inhibitory and excitatory neurotransmission. *Front. Cell. Neurosci.* 6:5. http://dx.doi.org/10.3389/fncel.2012.00005

Dopie, J., K.P. Skarp, E.K. Rajakylä, K. Tanhuanpää, and M.K. Vartiainen. 2012. Active maintenance of nuclear actin by importin 9 supports transcription. *Proc. Natl. Acad. Sci. USA.* 109:E544–E552. http://dx.doi.org/10.1073/pnas.1118880109

Edwards, D.C., L.C. Sanders, G.M. Bokoch, and G.N. Gill. 1999. Activation of LIM-kinase by Pak1 couples Rac/Cdc42 GTPase signalling to actin cytoskeletal dynamics. *Nat. Cell Biol.* 1:253–259. http://dx.doi.org/10.1038/12963

Ethell, I.M., and E.B. Pasquale. 2005. Molecular mechanisms of dendritic spine development and remodeling. *Prog. Neurobiol.* 75:161–205. http://dx.doi.org/10.1016/j.pneurobio.2005.02.003

Feng, G., R.H. Mellor, M. Bernstein, C. Keller-Peck, Q.T. Nguyen, M. Wallace, J.M. Nerbonne, J.W. Lichtman, and J.R. Sanes. 2000. Imaging neuronal subsets in transgenic mice expressing multiple spectral variants of GFP. *Neuron.* 28:41–51. http://dx.doi.org/10.1016/S0896-6273(00)00084-2

Fiumelli, H., A. Briner, M. Puskarjov, P. Blaesse, B.J. Belem, A.G. Dayer, K. Kaila, J.L. Martin, and L. Vutskits. 2013. An ion transport-independent role for the cation-chloride cotransporter KCC2 in dendritic spinogenesis in vivo. *Cereb. Cortex.* 23:378–388. http://dx.doi.org/10.1093/cercor/bhs027

Gauvain, G., I. Chamma, Q. Chevy, C. Cabezas, T. Irinopoulou, N. Bodrug, M. Carnaud, S. Lévi, and J.C. Poncer. 2011. The neuronal K-Cl cotransporter KCC2 influences postsynaptic AMPA receptor content and lateral diffusion in dendritic spines. *Proc. Natl. Acad. Sci. USA.* 108:15474–15479. http://dx.doi.org/10.1073/pnas.1107893108

Gulyás, A.I., A. Sík, J.A. Payne, K. Kaila, and T.F. Freund. 2001. The KCl cotransporter, KCC2, is highly expressed in the vicinity of excitatory synapses in the rat hippocampus. *Eur. J. Neurosci.* 13:2205–2217. http://dx.doi.org/10.1046/j.0953-816x.2001.01600.x

Honkura, N., M. Matsuzaki, J. Noguchi, G.C. Ellis-Davies, and H. Kasai. 2008. The subspine organization of actin fibers regulates the structure and plasticity of dendritic spines. *Neuron.* 57:719–729. http://dx.doi.org/10.1016/j.neuron.2008.01.013

Horn, Z., T. Ringstedt, P. Blaesse, K. Kaila, and E. Herlenius. 2010. Premature expression of KCC2 in embryonic mice perturbs neural development by an ion transport-independent mechanism. *Eur. J. Neurosci.* 31:2142–2155. http://dx.doi.org/10.1111/j.1460-9568.2010.07258.x

Hotulainen, P., and C.C. Hoogenraad. 2010. Actin in dendritic spines: connecting dynamics to function. *J. Cell Biol.* 189:619–629. http://dx.doi.org/10.1083/jcb.201003008

Hotulainen, P., E. Paunola, M.K. Vartiainen, and P. Lappalainen. 2005. Actin-depolymerizing factor and cofilin-1 play overlapping roles in promoting rapid F-actin depolymerization in mammalian nonmuscle cells. *Mol. Biol. Cell.* 16:649–664. http://dx.doi.org/10.1091/mbc.E04-07-0555

Hotulainen, P., O. Llano, S. Smirnov, K. Tanhuanpää, J. Faix, C. Rivera, and P. Lappalainen. 2009. Defining mechanisms of actin polymerization and depolymerization during dendritic spine morphogenesis. *J. Cell Biol.* 185:323–339. http://dx.doi.org/10.1083/jcb.200809046

Hübner, C.A., V. Stein, I. Hermans-Borgmeyer, T. Meyer, K. Ballanyi, and T.J. Jentsch. 2001. Disruption of KCC2 reveals an essential role of K-Cl cotransport already in early synaptic inhibition. *Neuron.* 30:515–524. http://dx.doi.org/10.1016/S0896-6273(01)00297-5

Ikeda, K., H. Onimaru, J. Yamada, K. Inoue, S. Ueno, T. Onaka, H. Toyoda, A. Arata, T.O. Ishikawa, M.M. Taketo, et al. 2004. Malfunction of respiratory-related neuronal activity in Na+, K+-ATPase alpha2 subunit-deficient mice is attributable to abnormal Cl- homeostasis in brainstem neurons. *J. Neurosci.* 24:10693–10701. http://dx.doi.org/10.1523/JNEUROSCI.2909-04.2004

Inoue, K., S. Ueno, and A. Fukuda. 2004. Interaction of neuron-specific K+-Cl- cotransporter, KCC2, with brain-type creatine kinase. *FEBS Lett.* 564:131–135. http://dx.doi.org/10.1016/S0014-5793(04)00328-X

Itoh, R.E., K. Kurokawa, Y. Ohba, H. Yoshizaki, N. Mochizuki, and M. Matsuda. 2002. Activation of rac and cdc42 video imaged by fluorescent resonance energy transfer-based single-molecule probes in the membrane of living cells. *Mol. Cell. Biol.* 22:6582–6591. http://dx.doi.org/10.1128/MCB.22.18.6582-6591.2002

Ivakine, E.A., B.A. Acton, V. Mahadevan, J. Ormond, M. Tang, J.C. Pressey, M.Y. Huang, D. Ng, E. Delpire, M.W. Salter, et al. 2013. Neto2 is a KCC2 interacting protein required for neuronal Cl- regulation in hippocampal neurons. *Proc. Natl. Acad. Sci. USA.* 110:3561–3566. http://dx.doi.org/10.1073/pnas.1212907110

Kim, S., T. Kim, D. Lee, S.H. Park, H. Kim, and D. Park. 2000. Molecular cloning of neuronally expressed mouse βPix isoforms. *Biochem. Biophys. Res. Commun.* 272:721–725. http://dx.doi.org/10.1006/bbrc.2000.2845

Koskinen, M., E. Bertling, and P. Hotulainen. 2012. Methods to measure actin treadmilling rate in dendritic spines. *Methods Enzymol.* 505:47–58. http://dx.doi.org/10.1016/B978-0-12-388448-0.00011-5

Li, H., S. Khirug, C. Cai, A. Ludwig, P. Blaesse, J. Kolikova, R. Afzalov, S.K. Coleman, S. Lauri, M.S. Airaksinen, et al. 2007. KCC2 interacts with the dendritic cytoskeleton to promote spine development. *Neuron.* 56:1019–1033. http://dx.doi.org/10.1016/j.neuron.2007.10.039

Ludwig, A., H. Li, M. Saarma, K. Kaila, and C. Rivera. 2003. Developmental up-regulation of KCC2 in the absence of GABAergic and glutamatergic transmission. *Eur. J. Neurosci.* 18:3199–3206. http://dx.doi.org/10.1111/j.1460-9568.2003.03069.x

Mahadevan, V., J.C. Pressey, B.A. Acton, P. Uvarov, M.Y. Huang, J. Chevrier, A. Puchalski, C.M. Li, E.A. Ivakine, M.S. Airaksinen, et al. 2014. Kainate receptors coexist in a functional complex with KCC2 and regulate chloride homeostasis in hippocampal neurons. *Cell Reports.* 7:1762–1770. http://dx.doi.org/10.1016/j.celrep.2014.05.022

Manser, E., T.H. Loo, C.G. Koh, Z.S. Zhao, X.Q. Chen, L. Tan, I. Tan, T. Leung, and L. Lim. 1998. PAK kinases are directly coupled to the PIX family of nucleotide exchange factors. *Mol. Cell.* 1:183–192. http://dx.doi.org/10.1016/S1097-2765(00)80019-2

Markkanen, M., T. Karhunen, O. Llano, A. Ludwig, C. Rivera, P. Uvarov, and M.S. Airaksinen. 2014. Distribution of neuronal KCC2a and KCC2b isoforms in mouse CNS. *J. Comp. Neurol.* 522:1897–1914. http://dx.doi.org/10.1002/cne.23510

Matus, A., M. Ackermann, G. Pehling, H.R. Byers, and K. Fujiwara. 1982. High actin concentrations in brain dendritic spines and postsynaptic densities. *Proc. Natl. Acad. Sci. USA.* 79:7590–7594. http://dx.doi.org/10.1073/pnas.79.23.7590

Medina, I., P. Friedel, C. Rivera, K.T. Kahle, N. Kourdougli, P. Uvarov, and C. Pellegrino. 2014. Current view on the functional regulation of the neuronal K(+)-Cl(-) cotransporter KCC2. *Front. Cell. Neurosci.* 8:27. http://dx.doi.org/10.3389/fncel.2014.00027

Meng, Y., Y. Zhang, V. Tregoubov, C. Janus, L. Cruz, M. Jackson, W.Y. Lu, J.F. MacDonald, J.Y. Wang, D.L. Falls, and Z. Jia. 2002. Abnormal spine morphology and enhanced LTP in LIMK-1 knockout mice. *Neuron.* 35:121–133. http://dx.doi.org/10.1016/S0896-6273(02)00758-4

Miller, J.H. 1972. Experiments in Molecular Genetics. Cold Spring Harbor Laboratory Press, Cold Spring Harbor, NY. 466 pp.

Mizuno, K. 2013. Signaling mechanisms and functional roles of cofilin phosphorylation and dephosphorylation. *Cell. Signal.* 25:457–469. http://dx.doi.org/10.1016/j.cellsig.2012.11.001

Nakayama, A.Y., M.B. Harms, and L. Luo. 2000. Small GTPases Rac and Rho in the maintenance of dendritic spines and branches in hippocampal pyramidal neurons. *J. Neurosci.* 20:5329–5338.

Park, E., M. Na, J. Choi, S. Kim, J.R. Lee, J. Yoon, D. Park, M. Sheng, and E. Kim. 2003. The Shank family of postsynaptic density proteins interacts with and promotes synaptic accumulation of the beta PIX guanine nucleotide exchange factor for Rac1 and Cdc42. *J. Biol. Chem.* 278:19220–19229. http://dx.doi.org/10.1074/jbc.M301052200

Payne, J.A., C. Rivera, J. Voipio, and K. Kaila. 2003. Cation-chloride co-transporters in neuronal communication, development and trauma. *Trends Neurosci.* 26:199–206. http://dx.doi.org/10.1016/S0166-2236(03)00068-7

Pellegrino, C., O. Gubkina, M. Schaefer, H. Becq, A. Ludwig, M. Mukhtarov, I. Chudotvorova, S. Corby, Y. Salyha, S. Salozhin, et al. 2011. Knocking down of the KCC2 in rat hippocampal neurons increases intracellular chloride concentration and compromises neuronal survival. *J. Physiol.* 589:2475–2496. http://dx.doi.org/10.1113/jphysiol.2010.203703

Penzes, P., and M.E. Cahill. 2012. Deconstructing signal transduction pathways that regulate the actin cytoskeleton in dendritic spines. *Cytoskeleton (Hoboken).* 69:426–441. http://dx.doi.org/10.1002/cm.21015

Pertz, O. 2010. Spatio-temporal Rho GTPase signaling - where are we now? *J. Cell Sci.* 123:1841–1850. http://dx.doi.org/10.1242/jcs.064345

Reynolds, A., E. Brustein, M. Liao, A. Mercado, E. Babilonia, D.B. Mount, and P. Drapeau. 2008. Neurogenic role of the depolarizing chloride gradient revealed by global overexpression of KCC2 from the onset of development. *J. Neurosci.* 28:1588–1597. http://dx.doi.org/10.1523/JNEUROSCI.3791-07.2008

Rivera, C., J. Voipio, J.A. Payne, E. Ruusuvuori, H. Lahtinen, K. Lamsa, U. Pirvola, M. Saarma, and K. Kaila. 1999. The K+/Cl- co-transporter KCC2 renders GABA hyperpolarizing during neuronal maturation. *Nature.* 397:251–255. http://dx.doi.org/10.1038/16697

Rodriguez, A., D.B. Ehlenberger, D.L. Dickstein, P.R. Hof, and S.L. Wearne. 2008. Automated three-dimensional detection and shape classification of dendritic spines from fluorescence microscopy images. *PLoS ONE.* 3:e1997. http://dx.doi.org/10.1371/journal.pone.0001997

Salin-Cantegrel, A., M. Shekarabi, S. Rasheed, F.M. Charron, J. Laganière, R. Gaudet, P.A. Dion, J.Y. Lapointe, and G.A. Rouleau. 2013. Potassium-chloride cotransporter 3 interacts with Vav2 to synchronize the cell volume decrease response with cell protrusion dynamics. *PLoS ONE.* 8:e65294. http://dx.doi.org/10.1371/journal.pone.0065294

Saneyoshi, T., and Y. Hayashi. 2012. The Ca2+ and Rho GTPase signaling pathways underlying activity-dependent actin remodeling at dendritic spines. *Cytoskeleton (Hoboken).* 69:545–554. http://dx.doi.org/10.1002/cm.21037

Saneyoshi, T., G. Wayman, D. Fortin, M. Davare, N. Hoshi, N. Nozaki, T. Natsume, and T.R. Soderling. 2008. Activity-dependent synaptogenesis: regulation by a CaM-kinase kinase/CaM-kinase I/βPIX signaling complex. *Neuron.* 57:94–107. http://dx.doi.org/10.1016/j.neuron.2007.11.016

Sarmiere, P.D., and J.R. Bamburg. 2004. Regulation of the neuronal actin cytoskeleton by ADF/cofilin. *J. Neurobiol.* 58:103–117. http://dx.doi.org/10.1002/neu.10267

Shi, Y., C.G. Pontrello, K.A. DeFea, L.F. Reichardt, and I.M. Ethell. 2009. Focal adhesion kinase acts downstream of EphB receptors to maintain mature dendritic spines by regulating cofilin activity. *J. Neurosci.* 29:8129–8142. http://dx.doi.org/10.1523/JNEUROSCI.4681-08.2009

Star, E.N., D.J. Kwiatkowski, and V.N. Murthy. 2002. Rapid turnover of actin in dendritic spines and its regulation by activity. *Nat. Neurosci.* 5:239–246. http://dx.doi.org/10.1038/nn811

Strange, K., T.D. Singer, R. Morrison, and E. Delpire. 2000. Dependence of KCC2 K-Cl cotransporter activity on a conserved carboxy terminus tyrosine residue. *Am. J. Physiol. Cell Physiol.* 279:C860–C867.

Takumi, Y., V. Ramírez-León, P. Laake, E. Rinvik, and O.P. Ottersen. 1999. Different modes of expression of AMPA and NMDA receptors in hippocampal synapses. *Nat. Neurosci.* 2:618–624. http://dx.doi.org/10.1038/10172

Tashiro, A., and R. Yuste. 2004. Regulation of dendritic spine motility and stability by Rac1 and Rho kinase: evidence for two forms of spine motility. *Mol. Cell. Neurosci.* 26:429–440. http://dx.doi.org/10.1016/j.mcn.2004.04.001

ten Klooster, J.P., Z.M. Jaffer, J. Chernoff, and P.L. Hordijk. 2006. Targeting and activation of Rac1 are mediated by the exchange factor β-Pix. *J. Cell Biol.* 172:759–769. http://dx.doi.org/10.1083/jcb.200509096

Tolias, K.F., J.G. Duman, and K. Um. 2011. Control of synapse development and plasticity by Rho GTPase regulatory proteins. *Prog. Neurobiol.* 94:133–148. http://dx.doi.org/10.1016/j.pneurobio.2011.04.011

Tornberg, J., V. Voikar, H. Savilahti, H. Rauvala, and M.S. Airaksinen. 2005. Behavioural phenotypes of hypomorphic KCC2-deficient mice. *Eur. J. Neurosci.* 21:1327–1337. http://dx.doi.org/10.1111/j.1460-9568.2005.03959.x

van Rheenen, J., M. Langeslag, and K. Jalink. 2004. Correcting confocal acquisition to optimize imaging of fluorescence resonance energy transfer by sensitized emission. *Biophys. J.* 86:2517–2529. http://dx.doi.org/10.1016/S0006-3495(04)74307-6

Wearne, S.L., A. Rodriguez, D.B. Ehlenberger, A.B. Rocher, S.C. Henderson, and P.R. Hof. 2005. New techniques for imaging, digitization and analysis of three-dimensional neural morphology on multiple scales. *Neuroscience.* 136:661–680. http://dx.doi.org/10.1016/j.neuroscience.2005.05.053

Wei, W.C., C.J. Akerman, S.E. Newey, J. Pan, N.W. Clinch, Y. Jacob, M.R. Shen, R.J. Wilkins, and J.C. Ellory. 2011. The potassium-chloride cotransporter 2 promotes cervical cancer cell migration and invasion by an ion transport-independent mechanism. *J. Physiol.* 589:5349–5359. http://dx.doi.org/10.1113/jphysiol.2011.214635

Zhang, H., D.J. Webb, H. Asmussen, and A.F. Horwitz. 2003. Synapse formation is regulated by the signaling adaptor GIT1. *J. Cell Biol.* 161:131–142. http://dx.doi.org/10.1083/jcb.200211002

Zhang, H., D.J. Webb, H. Asmussen, S. Niu, and A.F. Horwitz. 2005. A GIT1/PIX/Rac/PAK signaling module regulates spine morphogenesis and synapse formation through MLC. *J. Neurosci.* 25:3379–3388. http://dx.doi.org/10.1523/JNEUROSCI.3553-04.2005

Llano et al., http://www.jcb.org/cgi/content/full/jcb.201411008/DC1

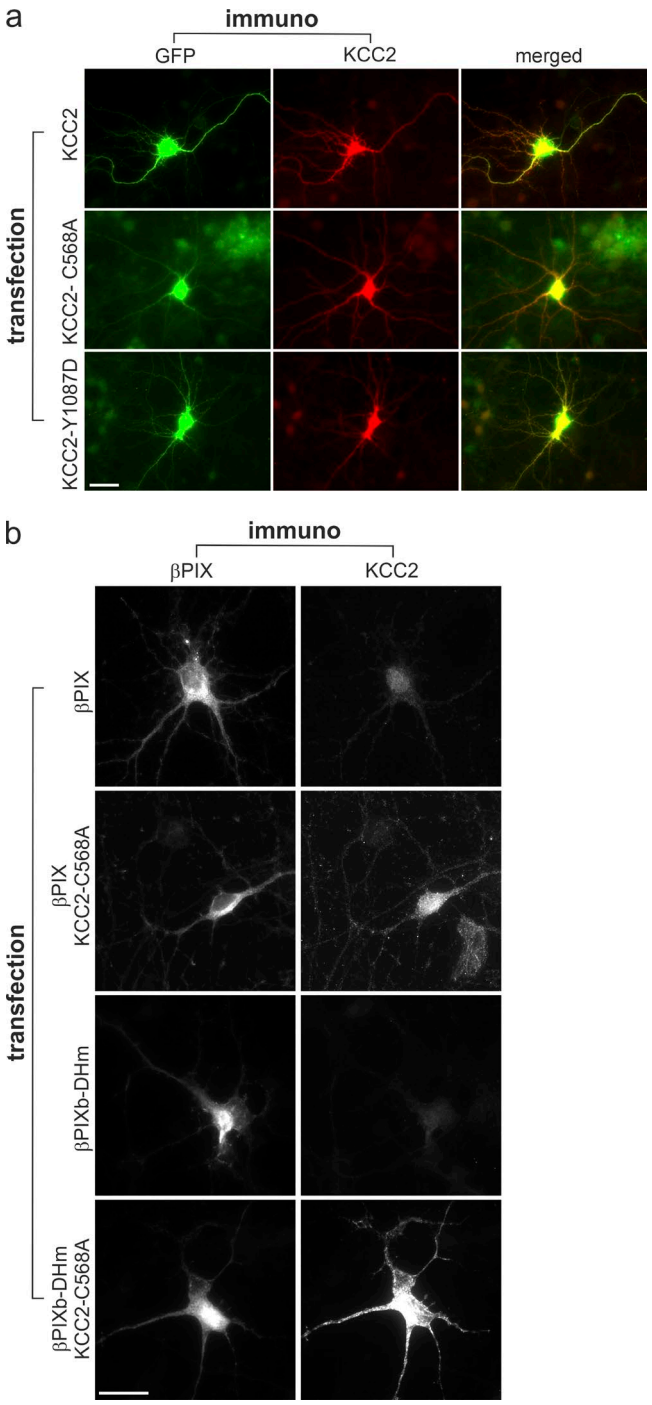

Figure S1. **Expression of chloride-transport-deficient KCC2 mutants in KCC2 KO neurons.** (a) Depictive immunostaining of GFP-transfected KCC2 KO neurons overexpressing KCC2, KCC2-C568A, and KCC2-Y1087D stained with antibodies against KCC2b (red). (b) Representative immunostaining of dissociated neurons transfected with β-PIX alone or with KCC2-C568A as well as β-PIX–DHm alone or with KCC2-C568A stained with antibodies against β-PIX and KCC2b. Bars, 20 µm.

a

Gal4 BD	Gal4 AD	LacZ
KCC1 (643-1085)	βPIXb (375-705)	+
KCC2b (644-1116)	βPIXb (375-705)	+++
KCC3a (677-1099)	βPIXb (375-705)	-
KCC4 (891-1340)	βPIXb (375-705)	+
NKCC1 (725-1203)	βPIXb (375-705)	-

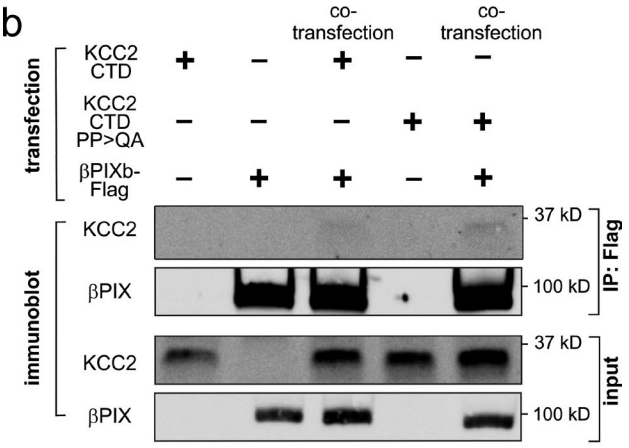

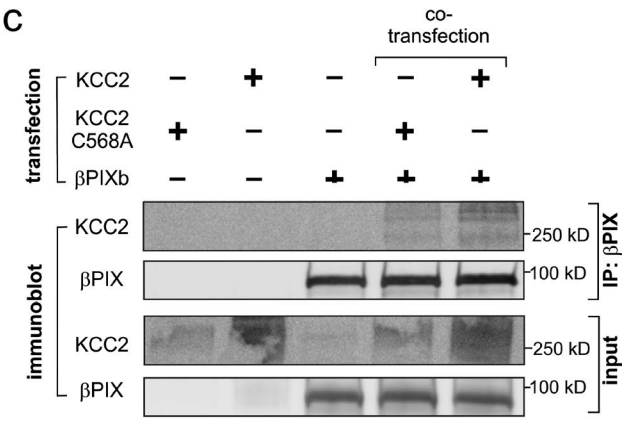

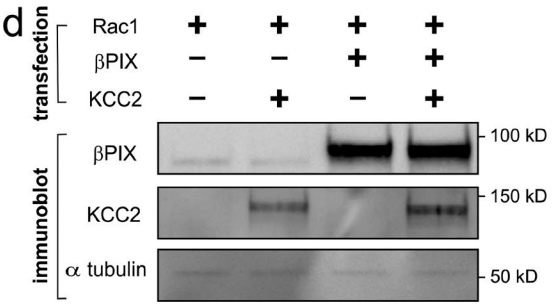

Figure S2. **Characterization of KCC2–β-PIX interaction and functional relevance.** (a) β-PIXb was isolated by yeast two-hybrid screening using the CTD of rat KCC2b as bait. Interactions with different members of the cation chloride cotransporter family were assessed by induction of the reporter gene LacZ after cotransfection of the respective baits (cation chloride cotransporters) with β-PIXb as prey. The optical density (OD600) was normalized to that of the control (cells transformed with mock vector). The relative optical density is denoted by symbols (from minimal to maximal: –, +, ++, +++). (b) Immunoblot of the immunoprecipitates obtained from HEK293T cell homogenates expressing β-PIXb–FLAG in combination with WT KCC2 CTD (aa 845–1,116) as well as the CTD containing the mutation in two proline-residues: P1077Q and P1078A using antibodies against FLAG-tag (IP: Flag) followed by immunoblot detection of KCC2. Both WT and mutant KCC2 CTDs were equally well coprecipitated with β-PIXb. (c) Immunoblot of the immunoprecipitates obtained from HEK293T cell homogenates expressing β-PIXb in combination with WT KCC2 as well as KCC2-C568A using antibodies against β-PIX (IP: β-PIX) followed by immunoblot detection of KCC2. Both WT and mutant KCC2 were equally well coprecipitated with β-PIXb. (d) Expression of β-PIX and KCC2 constructs in HEK293T cells in GLISA assay. Immunoblot of the HEK293T cell lysates used in the Rac1 activation assay (G-LISA assay) in Fig. 3 c.

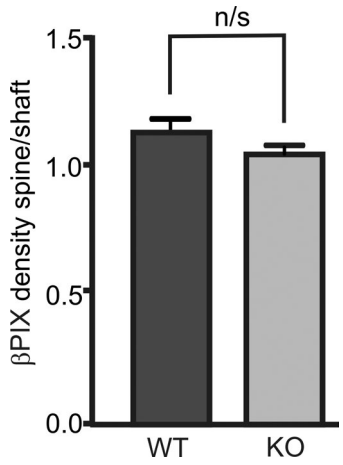

Figure S3. **Spine to shaft ratio of expression of β-PIX in KCC2-deficient neurons.** Quantification of density of immunostaining of β-PIX performed in cultured hippocampal neurons from KCC2-KO mice. The density of β-PIX in dendritic spines versus shafts was not significantly different in KCC2-deficient neurons compared with WT neurons (WT: 110 spines; KO: 118 spines; *t* test, P = 0.09; n/s, not significant). Error bars indicate SEM.